

## Effects of Overexpression of Fibroblast Growth Factor 15/19 on Hepatic Drug Metabolizing Enzymes

Daniel Rizzolo, Bo Kong, Stephanie Piekos, Liming Chen, Xiaobo Zhong, Jie Lu, Jian  
Shi, Hao-jie Zhu, Qian Yang, Albert Li, Linhao Li, Hongbing Wang, Anna  
Siemiątkowska, Celine Park, Leonid Kagan, Grace L. Guo

Department of Pharmacology and Toxicology, Ernest Mario School of Pharmacy (DR,  
BK, GLG), Department of Pharmaceutical Sciences, Ernest Mario School of Pharmacy  
(AS, CP, LK), Center of Excellence for Pharmaceutical Translational Research and  
Education (AS, CP, LK), Environmental and Occupational Health Sciences Institute  
(EOHSI) Rutgers University, Piscataway, NJ 08854 (DR, GLG); Rutgers Center for  
Lipid Research, Rutgers, The State University of New Jersey, New Brunswick, NJ  
08901 (DR, GLG); VA New Jersey Health Care System, Veterans Administration  
Medical Center, East Orange, NJ 07017 (GLG); Department of Pharmaceutical  
Sciences, University of Connecticut, Storrs, CT 06269 (SP, LC, XZ); Department of  
Pharmaceutical Sciences, School of Pharmacy, University of Pittsburgh, Pittsburgh,  
PA 15261 (JL); Department of Clinical Pharmacy, College of Pharmacy, University of  
Michigan, Ann Arbor, MI 48109 (JS, HZ); In Vitro ADMET Laboratories, LLC,  
Columbia, MD 21045 (QY, AL); Department of Pharmaceutical Sciences, School of  
Pharmacy, University of Maryland, Baltimore, MD 21201 (LL, HW); Department of  
Physical Pharmacy and Pharmacokinetics, Poznan University of Medical Sciences,  
Poznań 60-781, Poland (AS)

Corresponding Author: Grace L. Guo, MBBS, PhD, 170 Frelinghuysen Road,  
Piscataway, NJ, 08854 (address), (848)445-8186 (phone), (732)445-4161 (fax),  
guo@eohsi.rutgers.edu (e-mail)

**Key words:** FGF15, FXR, Bile acids, Drug metabolizing enzymes, growth hormone,  
sex difference

## Running Title

## Effects of Overexpression of FGF15/19 on Hepatic DMEs

Corresponding Author: Grace L. Guo, MBBS, PhD, 170 Frelinghuysen Road,  
Piscataway, NJ, 08854 (address), (848)445-8186 (phone), (732)445-4161 (fax),  
guo@eohsi.rutgers.edu (e-mail)

Text pages = 37

Tables = 0

Figures = 5

References = 29

Words in abstract = 248

Words in introduction = 750

Words in discussion = 924

## Abbreviations

Ad/EYFP-hCAR	Adenovirus expressing enhanced yellow fluorescent protein-tagged hCAR
BA	Bile acid
CAR	Constitutive androstane receptor
CAR <sup>-/-</sup>	CAR knockout mice
DMET	Drug metabolizing enzymes and transporters
ERK	Extracellular signal regulated kinase
FGF15	Fibroblast growth factor 15
<i>Fgf15</i> Tg	<i>Fgf15</i> transgenic mice
<i>Fgf15</i> <sup>int-/-</sup>	Intestine-specific <i>Fgf15</i> knockout mice
FGF19	Fibroblast growth factor 19
FGFR4	Fibroblast growth factor receptor 4
FXR	Farnesoid X receptor
GH	Growth hormone
HU	Hounsfield unit
JNK	c-Jun N-terminal kinase
MAPK	Mitogen-activated protein kinases

NAFLD	Non-alcoholic fatty liver diseases
NASH	Nonalcoholic steatohepatitis
NR	Nuclear receptor
PB	Phenobarbital
PHH	Primary human hepatocytes
RT-PCR	Real-time quantitative polymerase chain reaction
WT	Wild type



## Abstract

Fibroblast growth factor 15/19 (FGF15/19) are endocrine growth factors that play an important role in maintaining bile acid homeostasis. FGF15/19 based therapies are currently being tested in clinical trials for the treatment of non-alcoholic steatohepatitis and cholestatic liver diseases. To determine the physiological impact of long-term elevations of FGF15/19, a transgenic mouse model with overexpression of *Fgf15* (*Fgf15* Tg) was used in the current study. The RNA-seq analysis revealed elevations of the expression of several genes encoding phase I drug metabolizing enzymes (DMEs), including *Cyp2b10* and *Cyp3a11*, in *Fgf15* Tg mice. We found that the induction of several *Cyp2b* isoforms resulted in increased function of CYP2B in microsomal metabolism and pharmacokinetics studies. Because CYP2B family is known to be induced by constitutive androstane receptor (CAR), to determine the role of CAR in the observed inductions, we crossed *Fgf15* Tg mice with CAR knockout mice and found that CAR played a minor role in the observed alterations in DME expression. Interestingly, we found that the overexpression of *Fgf15* in male mice resulted in a phenotypical switch from the male hepatic expression pattern of DMEs to that of female mice. Differences in secretion of growth hormone (GH) between male and female mice are known to drive sexually dimorphic expression patterns of hepatic genes in a STAT5b dependent manner. We found that male *Fgf15* Tg mice presented with many features similar to GH deficiency, including lowered body length and weight, *Igf-1* and *Igfals* expression, and STAT5 signaling.

**Significance:** The overexpression of *Fgf15* in mice causes an alteration in DMEs at the mRNA, protein, and functional levels, which is not entirely due to CAR activation but associated with lower GH signaling.

## Introduction

Drug metabolism is the process by which exogenous compounds undergo biotransformation in order to facilitate their removal from the body. The process of drug metabolism is described in three phases: functional conversion, conjugation, and transport/excretion. The transcriptional regulation of genes encoding hepatic drug metabolizing enzymes and transporters (DMETs) is a critical mechanism capable of responding to various challenges during development, exposure to xenobiotics, and alterations in physiology and pathology.

The liver is the primary site of drug metabolism. The efficiency or rate at which the liver is able to process xenobiotic biotransformation is dependent upon the relative abundance of DMETs. In order to regulate the expression of DMETs, the liver is capable of responding to xenobiotic exposure through the activation of xenobiotic sensing nuclear receptors (NRs), such as the constitutive androstane receptor (CAR, NR1I3), pregnane X receptor, glucocorticoid receptor, and vitamin D receptor.

CAR is a well-studied xenobiotic sensing NR in the regulation of DMET gene expression. Under normal conditions, CAR is bound to the cytosol by a complex of heat-shock protein 90 and CAR cytoplasmic retention protein. Xenobiotics can activate CAR by both direct ligand binding and indirect protein modification mechanisms, causing dissociation from its chaperone proteins, followed by translocation to the nucleus (Mackowiak and Wang, 2016). Additionally, CAR is known to be inactivated by the androstane metabolites, androstenol and

androstanol, which act as inverse agonists (Kobayashi et al., 2015). Following translocation to the nucleus, CAR forms a heterodimer with the retinoid X receptor, binds to its response elements, and recruits co-activators SRC1 and GRIP1 to regulate target gene transcription (Mackowiak and Wang, 2016). CAR activation results in the differential regulation of over 2000 genes in mice and has overlap with pregnane X receptor and farnesoid X receptor (FXR, NR1H4) signaling (Cui and Klaassen, 2016). CAR activation is well known for mediating robust inductions of *CYP2B6* in humans and *Cyp2b10* in mice.

FXR is a NR that serves as a master regulator in bile acid (BA) homeostasis. BAs are amphipathic molecules that aid in the digestion and absorption of lipids and lipid-soluble vitamins in the small intestine. BAs are reabsorbed in the distal small bowel where they activate FXR to initiate a negative feedback mechanism, controlling their own synthesis (Makishima et al., 1999). Activation of intestinal FXR by BAs results in a strong induction of fibroblast growth factor 15 (FGF15) in mice and FGF19 in humans. FGF15/19 act as endocrine molecules, traveling to the liver where they interact with fibroblast growth factor receptor 4 (FGFR4) on hepatocytes. Activation of FGFR4 leads to the activation of the mitogen-activated protein kinases (MAPK) signaling pathway, including extracellular signal regulated kinase (ERK) and c-Jun N-terminal kinase (JNK), to reduce BA production by suppressing the expression of genes involved in BA synthesis, including *CYP7A1/Cyp7a1* and *CYP8B1/Cyp8b1* (Kong et al., 2012).

Many liver diseases are initiated and/or worsened by BA dysregulation, including cholestasis, non-alcoholic fatty liver diseases (NAFLD), and liver tumors (hepatocellular carcinoma and cholangiocarcinoma). Nonalcoholic steatohepatitis (NASH) is within the more severe spectrum of NAFLD, which includes liver steatosis and inflammation. Dysregulations of many of the metabolic pathways governed by FGF15/19 have been found to be sequelae of NASH. NASH is rapidly becoming a major health issue affecting approximately 3-12% of the US population (Spengler and Loomba, 2015) and is projected to overtake hepatitis C virus as the leading indication of liver transplant in the United States (Noureddin et al., 2018). Currently there are no approved drug therapies for the treatment of NASH but synthetic FXR ligands and modified FGF19 proteins are in clinical trials for the treatment of NASH and cholestatic liver diseases.

As pharmaceutical companies continue to investigate the potential of FXR agonism and FGF19 therapies for disease intervention, it is important to understand the long-term effects of these therapies on liver function. The impact of sustained elevations of plasma FGF15/19 protein on xenobiotic metabolism is unknown. Alterations to DMETs can lead to drug-drug interactions, in which a perpetrator drug alters the disposition and/or action of a victim drug when taken in combination. Drug-drug interactions can lead to the loss of efficacy or toxicity in patients, therefore it is important to properly evaluate the potential of new therapies to alter DMETs. In the current study, using the *Fgf15* transgenic mice (*Fgf15* Tg) and intestine-specific *Fgf15* knockout mice (*Fgf15*<sup>int-/-</sup>), as well as *in vitro*

synthesized FGF19 protein, we have determined the effect of modulating FGF15/19 levels on the hepatic expression and function of DMET genes. Additionally, using *in vitro* primary human hepatocytes (PHH) and *in vivo* CAR knockout mice (CAR<sup>-/-</sup>), we have examined the role of CAR in mediating the alterations of gene expression following FGF15/FGF19 overexpression.

## Materials and Methods

**Animals and Treatment.** Male 8-12 week old wild type (WT), *Fgf15* Tg, and *Fgf15*<sup>int-/-</sup> mice, all on C57BL/6J genetic background, were used (n=3-5). The generation of *Fgf15*<sup>int-/-</sup> mice is detailed in **Supplemental Fig. 4** and **Supplemental Doc. 1**. *Car*<sup>-/-</sup> mice on a mixed genetic background were generously gifted by Dr. Wen Xie from the University of Pittsburgh (Saini et al., 2004). F1 heterozygotes mice were obtained by crossing the *Car*<sup>-/-</sup> mice with *Fgf15* Tg mice, then intercross breeding of F1 heterozygotes was adapted to obtain genetic background matched WT, *Car*<sup>-/-</sup>, *Fgf15* Tg and *Car*<sup>-/-</sup>/*Fgf15* Tg mice. Male WT, *Car*<sup>-/-</sup>, *Fgf15* Tg and *Car*<sup>-/-</sup>/*Fgf15* were 12-16 weeks of age at time of necropsy. All animal experiments were performed according to protocols approved by the Institutional Animal Care and Use Committee (IACUC) at the Rutgers University. For positive controls of *Cyp2b10* and *Cyp3a11* induction in the liver, WT mice were IP injected with phenobarbital (PB, 50 mg/kg) for 3 days, and the control group was treated with PBS. All mice were euthanized for tissue collection between 10:00-11:00 AM without fasting. Methods for serum biochemical assays and liver histopathological examination have been described previously (Schumacher et al., 2020). Additional animal information can be found in **Supplemental Fig. 1**

**In vitro Treatment with Recombinant FGF19 Protein.** HepaRG cells were cultured as previously described (Hart et al., 2010; Pande et al., 2020). PHHs were from a cryopreserved pool (5 donors) of human hepatocytes (PHH8007A, IVAL, Columbia, MD). PHH were plated into a 6- or 24-well collagen coated plates at a

density of  $0.7 \times 10^6$  cells/ml and allowed to attach for 4 hours. Following attachment, plating medium was removed and the cells were changed to hepatocyte induction medium (HIM, IVAL, Columbia, MD). The plate was cultured in an incubator maintained with a humidified atmosphere of 95% air and 5% CO<sub>2</sub>. HepaRG and PHH were treated with recombinant FGF19 (Kong and Guo, 2014) at concentrations of 5 or 50 ng/ml for 24 and 48 hours. Recombinant FGF19 was diluted in PBS and PBS was used as the vehicle control.

**RNAseq Analysis.** Total liver RNA from WT, *Fgf15* Tg, or *Fgf15*<sup>int-/-</sup> male mice (n= 3 per group) was extracted from frozen tissue by TRIzol method (Thermo Fisher Scientific, Waltham, MA). Whole-transcriptome cDNA libraries were prepared by NuGEN Mondrian system. Paired-end sequencing was performed using the Illumina HiSeq 2000 platforms (Illumina, Inc., San Diego, CA). Alignment and read quantification were performed for all samples and FPKM values for each liver sample were calculated based on the method for RNAseq data analysis described previously (Peng et al., 2012).

**Gene Expression.** Relative gene expression was determined as previously described (Rizzolo et al., 2019). Briefly, total RNA was extracted from frozen liver or ileum tissue using TRIzol reagent. Reverse transcription was performed to acquire cDNA. Real-time quantitative polymerase chain reaction (RT-PCR) was performed on the ViiA7 Real Time PCR Machine (Life Technologies, Grand Island, NY) using SYBR green to determine relative gene expression. Ct values were



converted to delta delta Ct values and normalized to  $\beta$ -actin. Primer sequences used in this study can be found in **Supplementary Fig. 1**.

**Western Blot Analysis.** Livers were homogenized and lysed in 1X radioimmunoprecipitation assay buffer with protease and phosphatase inhibitors (Thermo Fisher Scientific, Waltham, MA). Proteins (20  $\mu$ g per well) were separated on a 10% sodium dodecyl sulphate-polyacrylamide gel and transferred to a polyvinylidene difluoride membrane. The blots were blocked for 2-hours at room temperature with 5% nonfat milk, incubated with primary antibody overnight at 4°C, incubated with species-specific secondary antibody for 1 hour at room temperature, and visualized using ECL substrates (Thermo Fisher Scientific, Waltham, MA). A list of antibodies used in this study can be found in **Supplemental Fig. 1**. Protein loading was normalized to levels of GAPDH or  $\beta$ -actin.

**CYP2B and CYP3A Enzyme Activity.** Liver microsomes were isolated from liver tissue, as previously described (Tien et al., 2015). Pentoxyresorufin and midazolam were used as probe substrates for the reactions pentoxyresorufin O-dealkylation and midazolam 1'-hydroxylation, which was used to detect the enzymatic activities of CYP2B and CYP3A, respectively. In brief, the incubation of 50  $\mu$ g of mouse liver microsomes was carried out in 1x phosphate-buffered saline (pH 7.4) with 30  $\mu$ M substrate concentration in a total volume of 95  $\mu$ L. The reactions were initiated with 5  $\mu$ L of 20 mM NADPH. Reactions containing pentoxyresorufin were carried out for 30 minutes and reactions containing midazolam were carried out for 10

minutes. All reactions were terminated by the addition of 100  $\mu$ L of ice-cold acetonitrile. The samples were vortexed for 30 seconds, centrifuged at 15,000 rpm for 10 minutes, and 1.0  $\mu$ L aliquots of the supernatant were injected into Waters Synapt G2-S QTOFMS system (Waters, Milford, MA) for metabolite analysis. Chromatographic separation of metabolites was performed on an Acquity UPLC BEH C18 column (2.1  $\times$  100 mm, 1.7  $\mu$ m, Waters). Details on the analytical methodology can be found in **Supplemental Doc. 1**.

**LC-MS/MS-based Protein Quantification.** Mouse liver microsome samples were digested for LC-MS/MS-based proteomic analysis as previously described (Shi et al., 2018). 80  $\mu$ g of protein from liver microsomes were mixed with 0.2  $\mu$ g of BSA internal standard. A detailed description of sample preparation and digestion can be found in **Supplemental Doc. 1**. The digested samples were analyzed on a TripleTOF 5600+ mass spectrometer (AB Sciex, Farmingham, MA) coupled with an Eksigent 2D plus LC system (Eksigent Technologies, Dublin, CA). LC separation was performed via a trap-elute configuration including a trapping column (ChromXP C18-CL, 120  $\text{\AA}$ , 5 $\mu$ m, 10  $\times$  0.3 mm, Eksigent Technologies, Dublin, CA) and an analytical column (ChromXP C18-CL, 120  $\text{\AA}$ , 150  $\times$  0.3 mm, 5 $\mu$ m, Eksigent Technologies, Dublin, CA). A detailed description of the analytical methodology can be found in **Supplemental Doc. 1**. The surrogate peptides used for quantification of CYP2B9, CYP2B10, CYP2B19, CYP3A11, CYP3A13, CYP3A16, and CYP3A25 are listed in **Supplemental Table 1**. These peptides were selected based on their uniqueness and chromatographic performance. The peak areas of top 3 to 5 fragment ions were

summed up and normalized to the internal standard BSA. The BSA-normalized peak area of each peptide was further divided by the average of the 18 samples to calculate the relative abundance of the peptide. The average of relative abundance of all surrogate peptides of a protein was used to determine the relative abundance across different microsome samples.

**CAR Nuclear Translocation by FGF19.** Adenovirus expressing enhanced yellow fluorescent protein-tagged hCAR (Ad/EYFP-hCAR) was used in PHHs (Bioreclamation In Vitro Technologies, Baltimore, MD). PHHs with over 90% viability were seeded at  $0.25 \times 10^6$  cells/well in 24-well biocoated plates in INVITROGRO™CP Medium (Bioreclamation In Vitro Technologies, Baltimore, MD) and infected with Ad/EYFP-hCAR (6  $\mu$ L/mL) as described previously (Li et al., 2009). Twenty-four hours after infection, PHHs were treated with vehicle control (0.1% DMSO), PB (1 mM), CITCO (1  $\mu$ M), or FGF19 (40 and 200 ng/mL) for 8h. EYFP-hCAR localization in hepatocytes was visualized on a Nikon Eclipse TI fluorescent microscope (Nikon, Melville, NY).

**Body Composition CT Imaging.** Male 5-month old WT and *Fgf15* Tg mice (n=5/group) were imaged using an Albira PET/CT (Bruker, Billerica, MA) as previously described (Metzinger et al., 2014; Murray et al., 2020). In brief, anesthetized mice were scanned using the following settings: Good Low High scan setting (400 slices), field of view (120mm<sup>2</sup>) with tube current (200  $\mu$ A) and voltage (45kV). After the scans were completed, they were reconstructed to a “Best” setting,

which increased the total slices to 600. The images were then analyzed using VivoQuant™ 2.0 imaging software. Hounsfield unit (HU) histograms were produced using 1000 bins describing a range of -1000 to 4000 HU. HU distribution was divided into three regions: fat (-350 to -75 HU), muscle (-75 to 200 HU), and bone (200 to 1000 HU). HU for each region was summed, divided by 512 (image matrix), corrected for bin total (1000), and then multiplied by tissue density factors of 0.9, 1.0, and 1.9 (g/cm<sup>3</sup>) for fat, muscle, and bone, respectively. To determine percent represented by each tissue, the previously described determination of mass was divided by the animal's body weight.

**Pharmacokinetic Study.** Male 4-month old WT and *Fgf15* Tg mice were injected I.V. with 1 mg/kg of bupropion (free base). Twenty µL of whole blood was collected with K<sub>3</sub>EDTA at 3, 30, 60, 120, 180, and 240 minutes. Samples were stored on ice and spun for 10 minutes at 10,000g for plasma collection. 10 µL of mouse K<sub>3</sub>EDTA plasma was spiked with 10 µL of a mixture of internal standards (250 ng/mL HBUP-D6 and 1000 ng/mL BUP-D9 in MeOH) and 10 µL of 10% trichloroacetic acid. Samples were vortexed for 5 min and centrifuged for 5 min at 10°C with 15 700 x *g*. The resulted supernatant was filtered through 0.2 µm PVDF filters at 10°C. The filtrate was then transferred to the HPLC vials with high-recovery inserts, and 10 µL was injected into the column. Bupropion and hydroxybupropion concentrations were determined by LC-MS/MS. A detailed description of the analytical methodology can be found in **Supplemental Doc. 1**. Pharmacokinetic parameters

were calculated by noncompartmental analysis with I.V. bolus dosing using PK Solver 2.0.

**Serum GH and IGF-1 ELISA Measurements.** Blood samples were collected every 30 mins from 9:30 am to 2:30 pm from WT and *Fgf15* Tg mice (male n = 5/genotype, female n = 3/genotype). In each collection, approximately 20  $\mu$ L of blood was collected from the lateral tail vein at each designated time point. After collection, blood samples were allowed to coagulate at room temperature for 10 mins, followed by centrifugation at 8000 g for 10 mins to prepare for serum. The serum samples were transferred to a fresh tube and stored at  $-80^{\circ}\text{C}$  until assay. Commercially available ELISA kits for growth hormone (GH) (EZRMGH-45K, Millipore-Sigma) and insulin-like growth factor-1 (IGF-1) (DY791, R&D Systems) were used to determine their levels in the serum. In order to reduce inter-sample dilution effects, serum samples were diluted identically 2 and 500 times before performing GH and IGF-1 ELISA assays, respectively. The sensitivities for the ELISA assays are 70 pg/ml and 3.5 pg/ml for GH and IGF-1, respectively.

**Statistical Analysis.** The data are presented as mean  $\pm$  1 SD. Groups were compared using a one-way ANOVA followed by Tukey post-hoc unless otherwise noted. Data that failed assumptions of parametric statistics were run as Kruskal-Wallis. Statistical analysis was run using SAS Studio. Data were considered significant at  $P$ -values  $< 0.05$ .

## Results

### Transcriptomes in FGF15 modified mouse livers

We have previously reported on the development of *Fgf15* Tg mice (Kong et al., 2018). The enterocyte-specific Fgf15 deficient mice (*Fgf15<sup>int-/-</sup>*) were generated in our laboratory by the recombineering technology (**Supplemental Fig. 4 and Supplemental Doc. 1**). In **Fig. 1A**, qPCR confirmed the overexpression of *Fgf15* in both the liver and ileum. The protein levels of FGF15 in serum of *Fgf15* Tg mice were markedly increased, while serum FGF15 levels in WT mice were undetectable as measured by a commercially available ELISA kit (data not shown). As expected, the overexpression of *Fgf15* resulted in a significant reduction of *Cyp7a1* mRNA levels. This reduction is a result of functional FGF15 binding to FGFR4 and not a result of hepatic FXR activation as these mice have significantly reduced levels of BAs (Kong et al., 2018) and there was no change in the hepatic expression of *FXR* or a classical FXR target gene, *Shp* (*Nr0b2*). In order to further understand transcriptional regulation affected by FGF15, we profiled the liver transcriptomes of WT, *Fgf15* Tg and *Fgf15<sup>int-/-</sup>* mice by RNA-seq analysis. Consistent with previous findings, the RNA-seq analysis (**Fig. 1B**) showed *Fgf15* Tg mice had reductions of the expression of hepatic genes involved in BA synthesis, such as *Cyp7a1* and *Cyp8b1*. *Fgf15<sup>int-/-</sup>* mice displayed slight inductions of *Cyp7a1* and *Cyp8b1*, likely due to reduced FGF15-FGFR4 binding. Amongst genes that were induced in *Fgf15* Tg mice were critical genes involved in phase I drug metabolism, such as *Cyp2b10*, *Cyp2b9*, and *Cyp3a11*.

## Gene and protein expression of hepatic drug metabolizing enzymes

RNA-seq analysis showed that the overexpression of *Fgf15* led to differential expression patterns for several cytochrome P450 genes involved in drug metabolism. **Fig. 2A** shows the validation of the observed induction of *Cyp2b9*, *Cyp2b10*, *Cyp3a11*, and *Cyp3a25* in *Fgf15* Tg mice at mRNA levels by RT-qPCR. Compared to WT mice, the mRNA levels of *Cyp2b9*, *Cyp2b10*, *Cyp3a11*, and *Cyp3a25* were all significantly increased in the livers of *Fgf15* Tg mice, with no significant changes to those in the livers of *Fgf15*<sup>int-/-</sup> mice. In order to determine if the observed alterations at the mRNA level were manifested at the protein level, we determined the protein expression of CYP2B and CYP3A in these mice by Western blots. Using antibodies targeting CYP2B and CYP3A, the results showed no change in the relative protein levels of CYP3A, an increase in CYP2B in *Fgf15* Tg mice but not in *Fgf15*<sup>int-/-</sup> mice, compared to WT mice (**Fig. 2B**).

## Determine the protein isoform expression by LC-MS/MS-based proteomics.

Because Western blot analysis can be limited in its ability to differentiate between cytochrome P450 isoforms, we further determined the protein levels of individual CYP2B and CYP3A family members via LC-MS/MS. **Fig. 2C** shows the effects of FGF15 modulation on individual CYP2B and CYP3A isoforms in the liver. In male WT mice, the predominately expressed CYP2B family members are CYP2B10 and CYP2B19, while CYP2B9 is undetectable as CYP2B9 is predominantly expressed in female mice. However, *Fgf15* Tg male mice showed marked inductions of CYP2B9, as compared to WT. *Fgf15*<sup>int-/-</sup> mice generally had less CYP2B protein, regardless of

isoform. Male WT mice had relatively equal amounts of CYP3A11, CYP3A13, and CYP3A25 while displaying no CYP3A16, which is generally found in neonates and female mice. *Fgf15*<sup>int-/-</sup> mice had minor reduction in CYP3A protein as compared to WT and also had no detectable CYP3A16. *Fgf15* Tg mice had about a 50% reduction in CYP3A11 protein despite showing an induction in *Cyp3a11* mRNA, as compared to WT mice. *Fgf15* Tg mice also had a slight reduction in CYP3A13 protein as compared to WT and a relatively similar amount of CYP3A25 protein. Interestingly, the *Fgf15* Tg mice did express CYP3A16 protein, which was not detected in the male WT mice.

### Functional activity of CYP2B and CYP3A enzymes

The functional activities of CYP2B and CYP3A were measured by treating isolated microsomes with the CYP2B and CYP3A probe substrates pentoxyresorufin and midazolam, respectively. Specifically, we measured the reactions of pentoxyresorufin O-dealkylation and midazolam 1'-hydroxylation by LC/MS, which was used to assess the enzymatic activities of CYP2B and CYP3A, respectively. Microsomes isolated from *Fgf15* Tg mice displayed a 1.70 fold increase in resorufin metabolite formation as compared to WT mice, suggesting the observed induction in CYP2B protein and mRNA resulted in an increase of CYP2B metabolic rate ( $P = 0.076$ ). Microsomes from *Fgf15*<sup>int-/-</sup> mice showed no significant change from WT with a fold change of 0.93, as compared to WT (**Fig. 2D**). PB-treated mice were used as a positive control and displayed a 6.41 fold increase in pentoxyresorufin O-dealkylation. There was no observed difference in the rate of midazolam



hydroxylation among WT, *Fgf15*<sup>int/-</sup>, and *Fgf15* Tg mice, suggesting there is no change to CYP3A hepatic microsomal activity.

### **FGF19 did not induce CYP2B and CYP3A in HepaRG or PHH cells**

We have previously described the successful production of soluble recombinant FGF19 protein (Kong and Guo, 2014). We used the recombinant FGF19 protein to treat HepaRG and PHH cells at concentrations of 5 ng/mL and 50 ng/mL for 24 and 48 hours. Although FGF19 treatment led to activation of FGFR4 pathway (data not shown), it did not induce the mRNA expression of *CYP2B6* or *CYP3A4* regardless of the cell type, concentration and time point (**Supplemental Fig. 2**).

### **Effects of FGF19 on CAR nuclear translocation *in vitro***

CAR is a classical xenobiotic sensing NR known to regulate the expression of many DMET genes. In order to determine whether FGF19 was capable of activating CAR in PHHs, an adenovirus expressing enhanced yellow fluorescent protein tagged hCAR (Ad/EYFP-hCAR) was used. Through the use of fluorescent microscopy, we were able to visualize the localization of the Ad/EYFP-hCAR following treatment with known activators of CAR (PB and CITCO) or recombinant FGF19 protein.

Following treatment with PB (1mM) or CITCO (1  $\mu$  M), the Ad/EYFP-hCAR translocated from the cytosol (diffuse YFP seen in the vehicle control group) to the nucleus. While the FGF19 (40 ng/mL or 200 ng/mL) treated PHHs showed almost no nucleus translocation of the Ad/EYFP-hCAR, as compared to the PB and CITCO

treated groups (**Fig 3A**). These data suggested that recombinant FGF19 protein could not activate CAR *in vitro*.

### **Effects of CAR on FGF15-alteration of DMET gene expression *in vivo***

Although FGF19 did not directly activate CAR *in vitro*, indirect activation of CAR *in vivo* remains a valid hypothesis. In order to determine the *in vivo* role of CAR on the observed inductions of drug metabolism genes in *Fgf15* Tg mice, we crossed *CAR*<sup>-/-</sup> mice with the *Fgf15* Tg mice to create *Fgf15* Tg/*CAR*<sup>-/-</sup> mice. These mice develop and breed normally. Serum assays in WT, *Fgf15* Tg, *CAR*<sup>-/-</sup>, and *Fgf15* Tg/*CAR*<sup>-/-</sup> mice showed no significant differences between groups for total cholesterol, triglycerides, or ALT, AST, or ALP activities (**Supplemental Fig. 3**). Liver histology was examined by a board certified pathologist. All WT and *Fgf15* Tg mice had no noteworthy findings. Most *Fgf15* Tg/*CAR*<sup>-/-</sup> mice displayed mild biliary hyperplasia. A detailed table of pathological findings can be found in **Supplemental Fig. 3**.

In **Fig. 3B** we measured the gene expression of 4 genes that are positively regulated by CAR activation (*Gsta1*, *Gstm3*, *Akr1b7*, *Cyp2b10*) and 3 genes that are negatively regulated by CAR activation (*Cyp2c55*, *Hsd3b5*, *Slco1a1*). Of genes positively regulated by CAR, *Fgf15* Tg mice displayed a  $2.07 \pm 1.17$  and  $1.93 \pm 0.82$  fold induction of *Gstm3* and *Akr1b7*, respectively, as compared to WT mice. *Fgf15* Tg/*CAR*<sup>-/-</sup> mice showed a slightly greater induction in the expression of *Gstm3* and *Akr1b7*, with a significant fold change of  $2.60 \pm 1.45$  and  $2.58 \pm 1.68$ , respectively. *Cyp2b10*, a prototypical CAR target gene is significantly induced  $12.46 \pm 6.11$  fold in

*Fgf15* Tg mice, as compared to WT mice. In *CAR*<sup>-/-</sup> mice, the expression of *Cyp2b10* was significantly reduced to  $0.16 \pm 0.16$ . In *Fgf15* Tg/*CAR*<sup>-/-</sup> mice *Cyp2b10* expression was significantly induced  $3.70 \pm 2.22$  fold as compared to WT, which is significantly less than that of the *Fgf15* Tg mice ( $P = 0.0004$ ). For genes negatively regulated by CAR activation, there was no significant difference in the expression of *Hsd3b5* or *Slco1a1* between WT and *CAR*<sup>-/-</sup> mice. However, *Fgf15* Tg mice displayed a significant reduction in *Hsd3b5* and *Slco1a1* mRNA expression of  $0.18 \pm 0.36$  and  $0.24 \pm 0.27$ , respectively. This reduction was further exacerbated in *Fgf15* Tg/*CAR*<sup>-/-</sup> mice to  $0.02 \pm 0.02$  and  $0.09 \pm 0.07$ , respectively, as compared to WT mice. In **Fig. 3C**, we measured the mRNA expression of 6 genes involved in phase I or phase II drug metabolism (*Cyp1a*, *Cyp3a11*, *Cyp3a16*, *Cyp3a44*, *Ugt1a1*, *Sult1a1*). There was no significant difference for any of the genes measured among WT, *CAR*<sup>-/-</sup>, *Fgf15* Tg, and *Fgf15* Tg/*CAR*<sup>-/-</sup> mice.

Amongst the differentially expressed cytochrome P450s described in **Figs. 1 & 2**, were *Cyp2b9* and *Cyp3a16*, which are known to have sexually dimorphic expression patterns, with both being expressed higher in female than in male mice. Using male WT, *Fgf15* Tg, *CAR*<sup>-/-</sup>, and *Fgf15* Tg/*CAR*<sup>-/-</sup> mice, we measured the relative expression of 6 genes that are predominantly expressed in male mice (**Fig. 3D**; *Hsd3b5*, *Ugt2b1*, *Srd5a1*, *Slco1a1*, *Mup1*, *Cyp2d9*) and the relative gene expression of 5 genes that are predominantly expressed in female mice (**Fig. 3E**; *Cyp2b9*, *Cyp2b13*, *Cyp17a1*, *Sult1e1*, *Hsd3b1*). *Fgf15* Tg mice displayed significant reductions in the expression of male dominant genes (**Fig. 3D**) *Hsd3b5*, *Ugt2b1*, *Slco1a1*, *Mup1*, and *Cyp2d9*, with

a trend towards a significant reduction of *Srd5a1* ( $P=0.0686$ ). There was no significant difference between WT and *CAR*<sup>-/-</sup> mice for any of the genes measured; however in *Fgf15* Tg/*CAR*<sup>-/-</sup> mice the significant reductions of male dominant genes in *Fgf15* Tg mice was further exacerbated in the absence of *CAR*. Male *Fgf15* Tg and *Fgf15* Tg/*CAR*<sup>-/-</sup> mice both displayed significant increases in the expression of *Cyp2b9*, *Cyp2b13*, and *Cyp17a1* with trends for increases in *Sult1e1* and *Hsd3b1* (**Fig. 3E**), genes that are predominantly expressed in female mice.

### **The impact of the overexpression of *Fgf15* on the pharmacokinetics of bupropion**

To assess the functional implications of the induction of CYP2B mRNA and protein in the *Fgf15* Tg mice, we performed a pharmacokinetic study using bupropion as a probe substrate to measure CYP2B activity *in vivo*. WT and *Fgf15* Tg mice were dosed with 1 mg/kg of bupropion I.V., plasma concentrations of bupropion and the metabolite hydroxybupropion were taken at 3, 30, 60, 120, 180, and 240 minutes. The mean plasma (nM) semi-logarithmic concentration time plots are shown in **Fig. 4A**. A summary table (**Fig. 4B**) shows that *Fgf15* Tg mice have a reduction ( $P=0.163$ ) in terminal half-life from 55.8 minutes to 46.8 minutes, as compared to WT. Additionally, *Fgf15* Tg mice displayed a higher C<sub>max</sub> of hydroxybupropion (18.1 ng/mL) than WT mice (13.4 ng/mL) mice and *Fgf15* Tg mice reached that maximum metabolite concentration 27.4 minutes faster ( $P=0.077$ ) than WT mice (a reduction of 28.5%). Taken together, these data suggest that *Fgf15* Tg mice convert

bupropion, a CYP2B probe substrate, to the metabolite hydroxybupropion at a faster rate than WT mice.

### Body size and composition

Gross observations suggested differences in the size of WT and *Fgf15* Tg mice (**Fig. 5A**). *Fgf15* Tg mice had a significantly shorter body length measured by nose-to-anus length ( $7.83 \pm 0.41\text{cm}$ ) than WT mice ( $9.15 \pm 0.42\text{cm}$ ). *Fgf15* Tg mice also weighed significantly less ( $22.45 \pm 2.18\text{g}$ ) than WT mice ( $27.98 \pm 0.94\text{g}$ ) (**Fig. 5B**). CT imaging was used to determine if the overexpression of *Fgf15* altered the disposition of fat, muscle, or bone (**Fig. 5C**). There were no noteworthy alterations in the distribution of fat, muscle or bone between WT mice (6.9%, 76.2%, and 16.0% respectively) and *Fgf15* Tg mice (7.4%, 74.0%, and 18.0% respectively).

### Cell signaling and growth hormone signaling pathways

FGFR4 activation by FGF15/19 is known to activate several intracellular signaling pathways, including ERK1/2-MAPK, PI3K-AKT, and JAK/STAT pathways (Liu et al., 2020). In **Fig. 5D**, we measured the modification of these pathways and semi-quantified the Western blot analysis. We observed an overall reduction in the phosphorylation of AKT, ERK, STAT3, and STAT5 in *Fgf15* Tg mice, as compared to WT. The reduction may be a result of desensitization to FGFR4 activation as a result of the continuous overexpression of *Fgf15*. Of note is the drastic reduction of phosphorylated STAT5 in 3 out of 4 *Fgf15* Tg samples measured. STAT5 signaling is well known to be activated by growth hormone and influence sexually dimorphic

hepatic gene expression patterns and growth development (Zhang et al., 2012; Martinez et al., 2013). Measurements of the mRNA levels of GH response genes, *Igf-1* and *Igfals*, showed reductions of gene expression in the livers of *Fgf15* Tg mice ( $P=0.068$  and  $0.085$ , respectively), as compared to WT mice (**Fig. 5E**).

### Serum Levels of GH and IGF-1

In order to assess potential differences in GH release between WT and *Fgf15* Tg mice, we collected blood from mice every 30 minutes from 9:30am to 2:30pm. In **Fig. 5F**, we measured the serum levels of GH and the GH response gene, IGF-1, via ELISA assays. WT mice generally displayed a typical male GH release pattern with a robust GH pulse beginning around 12:00 pm and reaching a maximum concentration around 12:30 pm. *Fgf15* Tg mice showed a GH release pattern more similar to female mice with low, steady levels detected. The serum GH levels for female mice were similar between WT and *Fgf15* Tg mice, with levels generally being maintained between 2-4 ng/mL (**Supplemental Fig. 5A**). Serum IGF-1 concentrations were more varied but WT mice tended to have higher levels of serum IGF-1 than *Fgf15* Tg mice.

### Discussion

FGF15 and its human orthologue FGF19 are endocrine FGFs that function to suppress BA production, reduce steatosis, regulate oxidative stress, promote liver growth and protein production, and improve insulin resistance in murine models of NASH (Henriksson and Andersen, 2020; Stofan and Guo, 2020). As such, FXR

agonists, which are capable of producing robust inductions of FGF15/19 through ileal FXR activation, as well as FGF19 analogs/mimetics, have been in clinical trials for the treatments of NASH and cholestatic liver diseases. In the present study, we determine the effects of FGF15/19 overexpression on DMETs *in vivo*, through the use of an *Fgf15* Tg mouse model, and *in vitro*, using recombinant FGF19 protein.

The overexpression of *Fgf15* caused a broad alteration of the expression of DMETs revealed by RNA-seq transcriptomic analysis. Alterations of DMETs can result in unintended clinical consequences, such as loss of efficacy or toxicity. For this reason, we wanted to explore the functional consequences of these alterations, as well as investigate the potential mechanisms underlying this regulation. Among the genes with their expression altered, we confirmed inductions of *Cyp2b9*, *Cyp2b10*, *Cyp3a11* and *Cyp3a25* at the mRNA level and inductions of CYP2B9, CYP2B10, CYP2B19, and CYP3A16 at the protein level as a result of the overexpression of *Fgf15*. Through the use of isolated hepatic microsomes from *Fgf15* Tg mice, we found an increase in the metabolism of pentoxoresorufin ( $P = 0.076$ ), a probe substrate for CYP2B activity. Our pharmacokinetic study also found an increase ( $P = 0.163$ ) in the rate of metabolism of bupropion, a CYP2B specific substrate, to the metabolite hydroxybupropion by *Fgf15* Tg mice, as compared to WT mice.

CAR is a well-studied xenobiotic sensing NR known to induce human CYP2B6 and CYP3A4 (CYP2B10 and CYP3A11 in mice). Recent research has shown a connection between FGF15 and FXR or CAR activation in a tissue specific manner (Weber et al.,

2021). In order to determine if the observed alterations in *Fgf15* Tg mice were a result of elevated CAR activation, we crossbred *Fgf15* Tg mice with *CAR*<sup>-/-</sup> mice to create *Fgf15* Tg/*CAR*<sup>-/-</sup> mice. We found that in some cases (*Gstm3* and *Akr1b7*), the loss of *CAR* exacerbated inductions brought about by the overexpression of *Fgf15*. In other cases (*Cyp2b10* and *Cyp17a1*), the loss of *CAR* attenuated inductions caused by the overexpression of *Fgf15*. Taken together, these data suggest *CAR* may play a role in altering the expression pattern of DMETs in mice overexpressing *Fgf15*; however, there are clearly additional mechanisms driving the observed alterations.

Amongst the phase I metabolizing enzymes that were induced in male *Fgf15* Tg mice was *Cyp2b9*. *Cyp2b9* is a sexually dimorphic cytochrome P450 that is predominantly expressed in female mice (Wiwi et al., 2004). Looking at other hepatic genes known to be sexually dimorphic, we found that male *Fgf15* Tg mice had large inductions of genes primarily expressed in the livers of female mice, e.g., *Cyp2b9*, *Cyp2b13*, *Cyp17a1*, *Sult1e1*, *Hsd3b1*. Conversely, we looked at the hepatic mRNA expression of male dominant genes and found that male *Fgf15* Tg mice had a significantly lower expression pattern of many of these genes, including *Hsd3b5*, *Ugt2b1*, *Slco1a1*, *Mup1*, and *Cyp2d9*.

STAT5 is a transcription factor activated predominately by growth hormone and plays a key role in the sexually dimorphic expression of cytochrome P450s in the liver (Davey et al., 1999). Neuroendocrine factors regulate a pulsatile (in male) or continual (in female) GH release, which, amongst other things, regulate the tyrosine



phosphorylation of STAT5b in the liver. In general, male mice go through cyclical periods of robust STAT5b phosphorylation/activation with periods of little or no activated STAT5b during the GH interpulse interval. Female mice have continual, low (but measurable) plasma GH and STAT5b activity (Waxman and O'Connor, 2006). Additionally, GH is known to influence body size and weight in mice (Kopchick et al., 2014). In line with this known mechanism of sexual dimorphism, our male *Fgf15* Tg mice exhibited a low consistent concentration of serum GH, while our male WT mice displayed the prototypical male GH surge. As a likely result of altered GH signaling, our *Fgf15* Tg mice had greatly reduced STAT5 phosphorylation as compared to WT mice. Downstream measurements of GH response genes *Igf-1* and *Igfals* showed reduced mRNA expression in the livers of *Fgf15* Tg mice ( $P=0.068$  and  $0.085$ , respectively). Additionally, *Fgf15* Tg mice have a shorter nose to anus length and reduced body weight compared to WT mice. Factors known to impact GH secretion patterns include stress, exercise, nutritional state, and metabolic signals (Kato et al., 2002). The observed alterations could be a result of reduced BAs impacting lipid and lipid-soluble vitamin absorption, causing changes to the nutritional state or metabolic signaling in the *Fgf15* Tg mice. The impact of FGF15/19 on GH regulation and STAT5b activity is the subject of an ongoing investigation in our lab.

The influence of FXR and BAs in liver disease etiology is well established. As pharmaceutical companies continue to probe the FXR-BA-FGF15/19 pathway for the therapeutic intervention in treating diseases associated with BA dysregulation,

it is important to understand the potential that manipulating these pathways have on the regulation of drug metabolizing enzymes. Through the use of an *Fgf15* Tg mouse model, we have shown that the overexpression of *Fgf15* induces the expression of several phase I metabolizing enzymes and leads to a phenotypical switch from a male to female expression pattern in the livers of male *Fgf15* Tg mice. The mechanism underlying this gender switch is unclear. However, the *Fgf15* Tg mice have much lower BA contents than WT mice, which negatively affect lipid absorption. Lower lipid absorption is a form a nutrient deprivation known to be associated with growth retardation. In our study, we found shorter body length, reduced STAT5 activation, altered serum GH levels, and reduced GH target gene expression (*Igf-1* and *Igfals*) as a result of *Fgf15* overexpression. GH reduction may lead to CAR activation by releasing factors known to inhibit CAR activation, including EGFR signaling and production of CAR endogenous inhibitors. We will further determine the underling mechanism in future studies to determine the extent to which reduced GH and STAT5 signaling is responsible for the observed gender specific switch of DMET expression.

In summary, we have shown that overexpression of FGF15 led to a gender specific switch of the expression of genes encoding DMETs in the liver. The mechanism responsible for this switch is unclear; however, initial data from the studies suggest that reduced GH signaling and increased CAR activation are associated with this switch.

## Figure Captions

**Fig. 1 Relative hepatic and ileal mRNA values of Fgf15 related genes and RNAseq analysis.** (A) Hepatic and ileal gene expression was normalized to  $\beta$ -actin mRNA expression and graphs depict relative mRNA  $\pm$  1 SD (n: WT= 9, *Fgf15*<sup>int-/-</sup>= 6, *Fgf15* Tg= 5; one-way ANOVA, Tukey post-hoc). An asterisk denotes a significant difference from WT ( $P < 0.05$ ). (B) Heat map illustrates log2 fold-change in RNAseq analysis as compared to WT (n=3/group).

**Fig. 2 Relative hepatic mRNA, protein, and function of cytochrome P450s.** (A) Relative hepatic mRNA expression normalized to  $\beta$ -actin mRNA expression (n: WT= 5, *Fgf15*<sup>int-/-</sup>= 6, *Fgf15* Tg= 5; one-way ANOVA, Tukey post-hoc). Graphs depict relative mRNA  $\pm$  1 SD. An asterisk denotes a significant difference from WT ( $P < 0.05$ ). *Cyp2b9* and *Cyp2b10* failed Levene's test therefore Kruskal-Wallis was used for analysis. (B) Western blot of CYP3A and CYP2B using 20 $\mu$ g of liver homogenate (n: WT= 4, *Fgf15*<sup>int-/-</sup>= 5, *Fgf15* Tg= 5; one-way ANOVA, Tukey post-hoc). (C) LCMS analysis of relative protein expression of CYP2B and CYP3A isoforms (n: WT= 5, *Fgf15*<sup>int-/-</sup>= 5, *Fgf15* Tg= 5, WT-PB= 3; one-way ANOVA, Tukey post-hoc). . (D) Measurements of pentoxyresorufin and midazolam metabolite formation to assess CYP2B and CYP3A activity in liver microsomes of WT, *Fgf15*<sup>int-/-</sup>, *Fgf15* Tg, and phenobarbital treated WT mice (n: WT= 5, *Fgf15*<sup>int-/-</sup>= 5, *Fgf15* Tg= 5, WT-PB= 3; one-way ANOVA, Tukey post-hoc).

**Fig. 3 Role of CAR in alterations brought about by the overexpression of *Fgf15/19*.** (A) Fluorescent imaging of Ad/EYFP-hCAR PHHs treated with PB, CITCO, or FGF19 recombinant protein. (B-E) Hepatic gene expression was normalized to  $\beta$ -actin mRNA expression and graphs depict relative mRNA  $\pm$  1 SD. An asterisk denotes a significant difference from WT ( $P < 0.05$ ). *Cyp2b10*, *Cyp2b9*, *Cyp2b13*, and *Cyp17a1* failed Levene's test therefore Kruskal-Wallis was used for analysis. (B) Relative hepatic mRNA expression of genes regulated by CAR. (C) Relative hepatic mRNA expression of genes involved in drug metabolism. (D) Relative hepatic mRNA expression of genes predominantly expressed in male mice. (E) Relative hepatic mRNA expression of genes predominantly expressed in female mice (n: WT= 6, *Fgf15* Tg= 7, CAR<sup>-/-</sup>= 6, *Fgf15* Tg/CAR<sup>-/-</sup>= 7; one-way ANOVA, Tukey post-hoc).

**Fig. 4 Impact of *Fgf15* overexpression on the pharmacokinetics of bupropion in mouse plasma.** (A) Average log concentrations of bupropion and hydroxybupropion (+SD) in wild type and *Fgf15* Tg mouse plasma. (B) Table summarizing pharmacokinetic parameters ( $\pm$  SD) of bupropion and hydroxybupropion in wild type and *Fgf15* Tg mouse plasma (n: WT= 10, *Fgf15* Tg= 8; Student's *t*-test).

**Fig. 5 Body size and composition of WT and *Fgf15* Tg mice.** (A) Representative dorsal view of WT (top) and *Fgf15* Tg (bottom) mice. (B) Quantification of nose to anus length (cm) and body weight (g) of WT and *Fgf15* Tg mice (n: WT= 5, *Fgf15* Tg= 6; Student's *t*-test). (C) Percent of total body weight distributed as fat, muscle, and

bone (n: WT= 5, *Fgf15* Tg= 5; Student's *t*-test). (D) Western blots and semiquantifications of cell signaling proteins in liver homogenates from WT and *Fgf15* Tg mice (n: WT= 4, *Fgf15* Tg= 4). (E) Relative hepatic gene expression of GH response genes *Igf-1* and *Igfals* (n: WT= 6, *Fgf15* Tg= 7; Student's *t*-test). (F) Serum GH (left) and IGF-1 (right) levels in WT and *Fgf15* Tg mice measured by ELISA every 30 minutes from 9:30am to 2:30pm.

## Acknowledgements

We are grateful to Dr. Wen Xie for graciously providing CAR knockout mice. We appreciate the technical support by Miss. Katherine Otersen.

## Authorship Contributions

*Participated in research design:* Rizzolo, Kong, Guo

*Conducted experiments:* Rizzolo, Kong, Piekos, Chen, Lu, Siemiątkowska, Yang, A Li, L Li, Park, Shi

*Contributed new reagents or analytical tools:* Kagan, Guo

*Performed data analysis:* Rizzolo, Kong, Piekos, Siemiątkowska, Zhu, Zhong, Wang, Guo

*Wrote or contributed to the writing of the manuscript:* Rizzolo, Guo

## References

- Cui JY and Klaassen CD (2016) RNA-Seq reveals common and unique PXR- and CAR-target gene signatures in the mouse liver transcriptome. *Biochimica et biophysica acta* **1859**:1198-1217.
- Davey HW, Wilkins RJ, and Waxman DJ (1999) STAT5 signaling in sexually dimorphic gene expression and growth patterns. *Am J Hum Genet* **65**:959-965.
- Hart SN, Li Y, Nakamoto K, Subileau EA, Steen D, and Zhong XB (2010) A comparison of whole genome gene expression profiles of HepaRG cells and HepG2 cells to primary human hepatocytes and human liver tissues. *Drug Metab Dispos* **38**:988-994.
- Henriksson E and Andersen B (2020) FGF19 and FGF21 for the Treatment of NASH—Two Sides of the Same Coin? Differential and Overlapping Effects of FGF19 and FGF21 From Mice to Human. *Frontiers in Endocrinology* **11**.
- Kato Y, Murakami Y, Sohmiya M, and Nishiki M (2002) Regulation of Human Growth Hormone Secretion and Its Disorders. *Internal Medicine* **41**:7-13.
- Kobayashi K, Hashimoto M, Honkakoski P, and Negishi M (2015) Regulation of gene expression by CAR: an update. *Archives of Toxicology* **89**:1045-1055.
- Kong B and Guo GL (2014) Soluble expression of disulfide bond containing proteins FGF15 and FGF19 in the cytoplasm of Escherichia coli. *PLoS One* **9**:e85890.
- Kong B, Sun R, Huang M, Chow MD, Zhong XB, Xie W, Lee YH, and Guo GL (2018) Fibroblast Growth Factor 15-Dependent and Bile Acid-Independent Promotion of Liver Regeneration in Mice. *Hepatology* **68**:1961-1976.
- Kong B, Wang L, Chiang JY, Zhang Y, Klaassen CD, and Guo GL (2012) Mechanism of tissue-specific farnesoid X receptor in suppressing the expression of genes in bile-acid synthesis in mice. *Hepatology* **56**:1034-1043.
- Kopchick JJ, List EO, Kelder B, Gosney ES, and Berryman DE (2014) Evaluation of growth hormone (GH) action in mice: discovery of GH receptor antagonists and clinical indications. *Molecular and cellular endocrinology* **386**:34-45.
- Li H, Chen T, Cottrell J, and Wang H (2009) Nuclear translocation of adenoviral-enhanced yellow fluorescent protein-tagged-human constitutive androstane receptor (hCAR): a novel tool for screening hCAR activators in human primary hepatocytes. *Drug Metab Dispos* **37**:1098-1106.
- Liu P, Jenkins NA, and Copeland NG (2003) A highly efficient recombineering-based method for generating conditional knockout mutations. *Genome Res* **13**:476-484.
- Liu Y, Cao M, Cai Y, Li X, Zhao C, and Cui R (2020) Dissecting the Role of the FGF19-FGFR4 Signaling Pathway in Cancer Development and Progression. *Frontiers in cell and developmental biology* **8**:95-95.
- Mackowiak B and Wang H (2016) Mechanisms of xenobiotic receptor activation: Direct vs. indirect. *Biochim Biophys Acta* **1859**:1130-1140.
- Makishima M, Okamoto AY, Repa JJ, Tu H, Learned RM, Luk A, Hull MV, Lustig KD, Mangelsdorf DJ, and Shan B (1999) Identification of a nuclear receptor for bile acids. *Science* **284**:1362-1365.

- Martinez CS, Piazza VG, Ratner LD, Matos MN, González L, Rulli SB, Miquet JG, and Sotelo AI (2013) Growth hormone STAT5-mediated signaling and its modulation in mice liver during the growth period. *Growth Horm IGF Res* **23**:19-28.
- Metzinger MN, Miramontes B, Zhou P, Liu Y, Chapman S, Sun L, Sasser TA, Duffield GE, Stack MS, and Leevy WM (2014) Correlation of X-ray computed tomography with quantitative nuclear magnetic resonance methods for pre-clinical measurement of adipose and lean tissues in living mice. *Sensors (Basel, Switzerland)* **14**:18526-18542.
- Murray A, Gow AJ, Venosa A, Andres J, Malaviya R, Adler D, Yurkow E, Laskin JD, and Laskin DL (2020) Assessment of mustard vesicant lung injury and anti-TNF- $\alpha$  efficacy in rodents using live-animal imaging. *Ann N Y Acad Sci* **1480**:246-256.
- Nouredin M, Vipani A, Bresee C, Todo T, Kim IK, Alkhouri N, Setiawan VW, Tran T, Ayoub WS, Lu SC, Klein AS, Sundaram V, and Nissen NN (2018) NASH Leading Cause of Liver Transplant in Women: Updated Analysis of Indications For Liver Transplant and Ethnic and Gender Variances. *Am J Gastroenterol* **113**:1649-1659.
- Pande P, Zhong XB, and Ku WW (2020) Histone Methyltransferase G9a Regulates Expression of Nuclear Receptors and Cytochrome P450 Enzymes in HepaRG Cells at Basal Level and in Fatty Acid Induced Steatosis. *Drug Metab Dispos* **48**:1321-1329.
- Peng L, Yoo B, Gunewardena SS, Lu H, Klaassen CD, and Zhong X-B (2012) RNA sequencing reveals dynamic changes of mRNA abundance of cytochromes P450 and their alternative transcripts during mouse liver development. *Drug metabolism and disposition: the biological fate of chemicals* **40**:1198-1209.
- Rizzolo D, Buckley K, Kong B, Zhan L, Shen J, Stofan M, Brinker A, Goedken M, Buckley B, and Guo GL (2019) Bile Acid Homeostasis in a Cholesterol 7 $\alpha$ -Hydroxylase and Sterol 27-Hydroxylase Double Knockout Mouse Model. *Hepatology* **70**:389-402.
- Saini SPS, Sonoda J, Xu L, Toma D, Uppal H, Mu Y, Ren S, Moore DD, Evans RM, and Xie W (2004) A Novel Constitutive Androstane Receptor-Mediated and CYP3A-Independent Pathway of Bile Acid Detoxification. *Molecular Pharmacology* **65**:292-300.
- Schumacher JD, Kong B, Wu J, Rizzolo D, Armstrong LE, Chow MD, Goedken M, Lee Y-H, and Guo GL (2020) Direct and Indirect Effects of Fibroblast Growth Factor (FGF) 15 and FGF19 on Liver Fibrosis Development. *Hepatology* **71**:670-685.
- Shi J, Wang X, Lyu L, Jiang H, and Zhu HJ (2018) Comparison of protein expression between human livers and the hepatic cell lines HepG2, Hep3B, and Huh7 using SWATH and MRM-HR proteomics: Focusing on drug-metabolizing enzymes. *Drug Metab Pharmacokinet* **33**:133-140.
- Spengler EK and Loomba R (2015) Recommendations for Diagnosis, Referral for Liver Biopsy, and Treatment of Nonalcoholic Fatty Liver Disease and Nonalcoholic Steatohepatitis. *Mayo Clinic Proceedings* **90**:1233-1246.
- Stofan M and Guo GL (2020) Bile Acids and FXR: Novel Targets for Liver Diseases. *Frontiers in Medicine* **7**.



- Tien Y-C, Liu K, Pope C, Wang P, Ma X, and Zhong X-b (2015) Dose of Phenobarbital and Age of Treatment at Early Life are Two Key Factors for the Persistent Induction of Cytochrome P450 Enzymes in Adult Mouse Liver. *Drug Metabolism and Disposition* **43**:1938-1945.
- Waxman DJ and O'Connor C (2006) Growth Hormone Regulation of Sex-Dependent Liver Gene Expression. *Molecular Endocrinology* **20**:2613-2629.
- Weber AA, Mennillo E, Yang X, van der Schoor LWE, Jonker JW, Chen S, and Tukey RH (2021) Regulation of Intestinal UDP-Glucuronosyltransferase 1A1 by the Farnesoid X Receptor Agonist Obeticholic Acid Is Controlled by Constitutive Androstane Receptor through Intestinal Maturation. *Drug Metabolism and Disposition* **49**:12-19.
- Wiwi CA, Gupte M, and Waxman DJ (2004) Sexually dimorphic P450 gene expression in liver-specific hepatocyte nuclear factor 4alpha-deficient mice. *Mol Endocrinol* **18**:1975-1987.
- Liu P, Jenkins NA, and Copeland NG (2003) A highly efficient recombineering-based method for generating conditional knockout mutations. *Genome Res* **13**:476-484.
- Tien Y-C, Liu K, Pope C, Wang P, Ma X, and Zhong X-b (2015) Dose of Phenobarbital and Age of Treatment at Early Life are Two Key Factors for the Persistent Induction of Cytochrome P450 Enzymes in Adult Mouse Liver. *Drug Metabolism and Disposition* **43**:1938-1945.
- Wright TJ, Ladher R, McWhirter J, Murre C, Schoenwolf GC, and Mansour SL (2004) Mouse FGF15 is the ortholog of human and chick FGF19, but is not uniquely required for otic induction. *Dev Biol* **269**:264-275.
- Zhang Y, Laz EV, and Waxman DJ (2012) Dynamic, sex-differential STAT5 and BCL6 binding to sex-biased, growth hormone-regulated genes in adult mouse liver. *Mol Cell Biol* **32**:880-896.

## Footnotes

This work was supported by the National Institutes of Health [GM135258, ES029258, DK122725]; the VA [BX002741]; and the Rutgers Center for Lipid Research graduate student small grant award.

Part of this work was presented in the doctoral dissertation of D. Rizzolo (2021): *Regulation of hepatic drug metabolizing enzymes by the bile acid-FXR- FGF15/19 pathway.*

The authors declare that they have no conflicts of interest with the contents of this article.

Figure 1

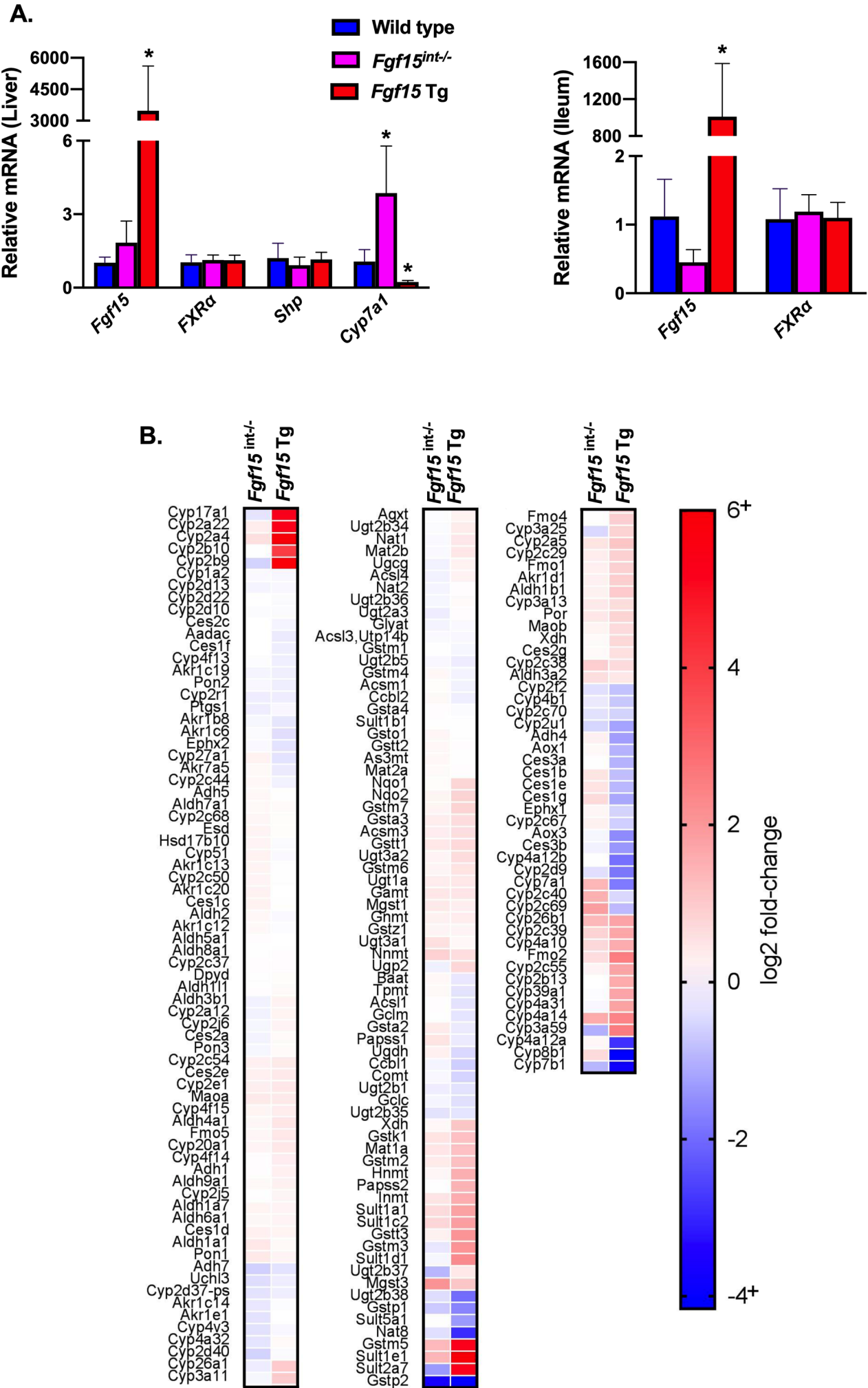
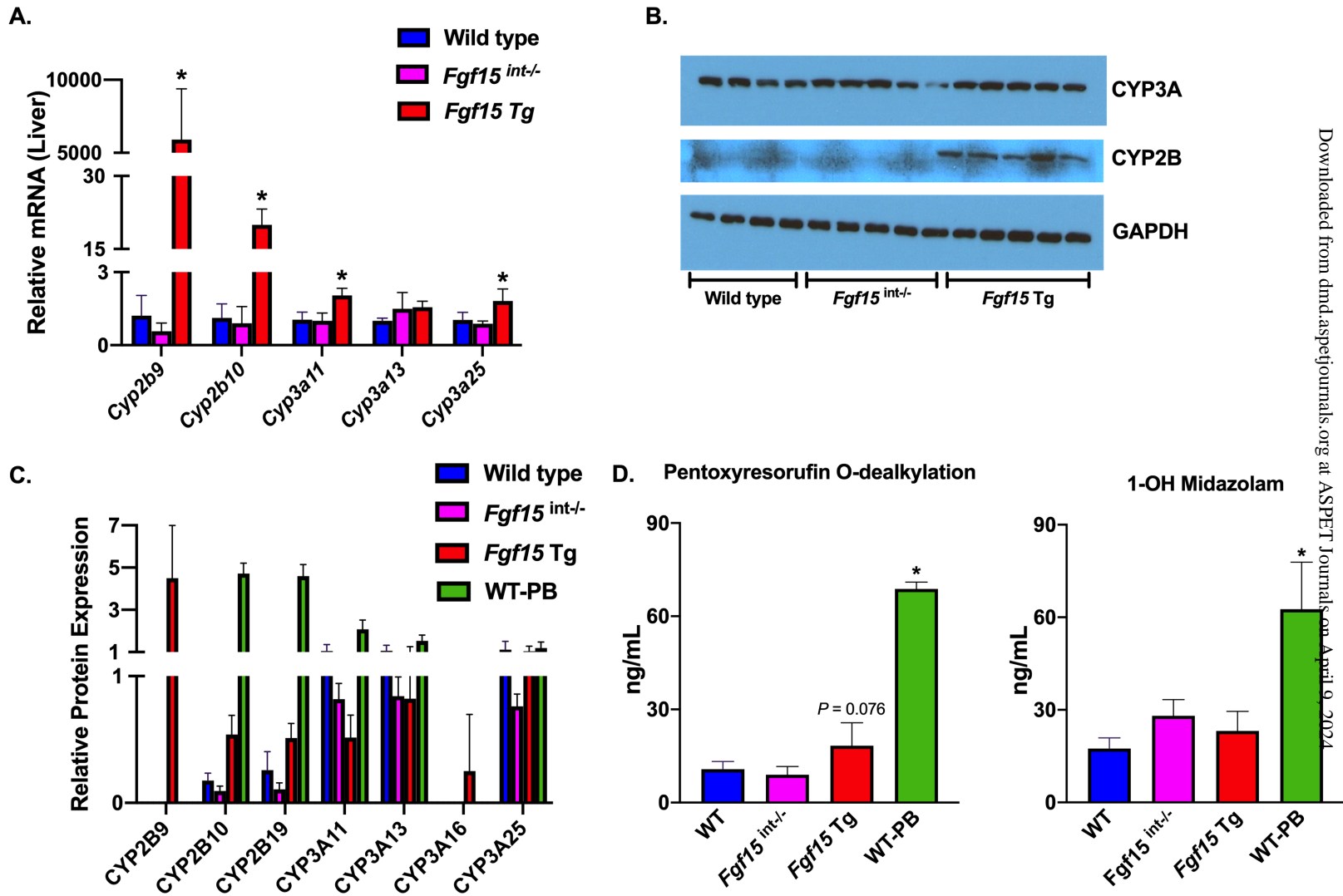


Figure 2



**Figure 3**

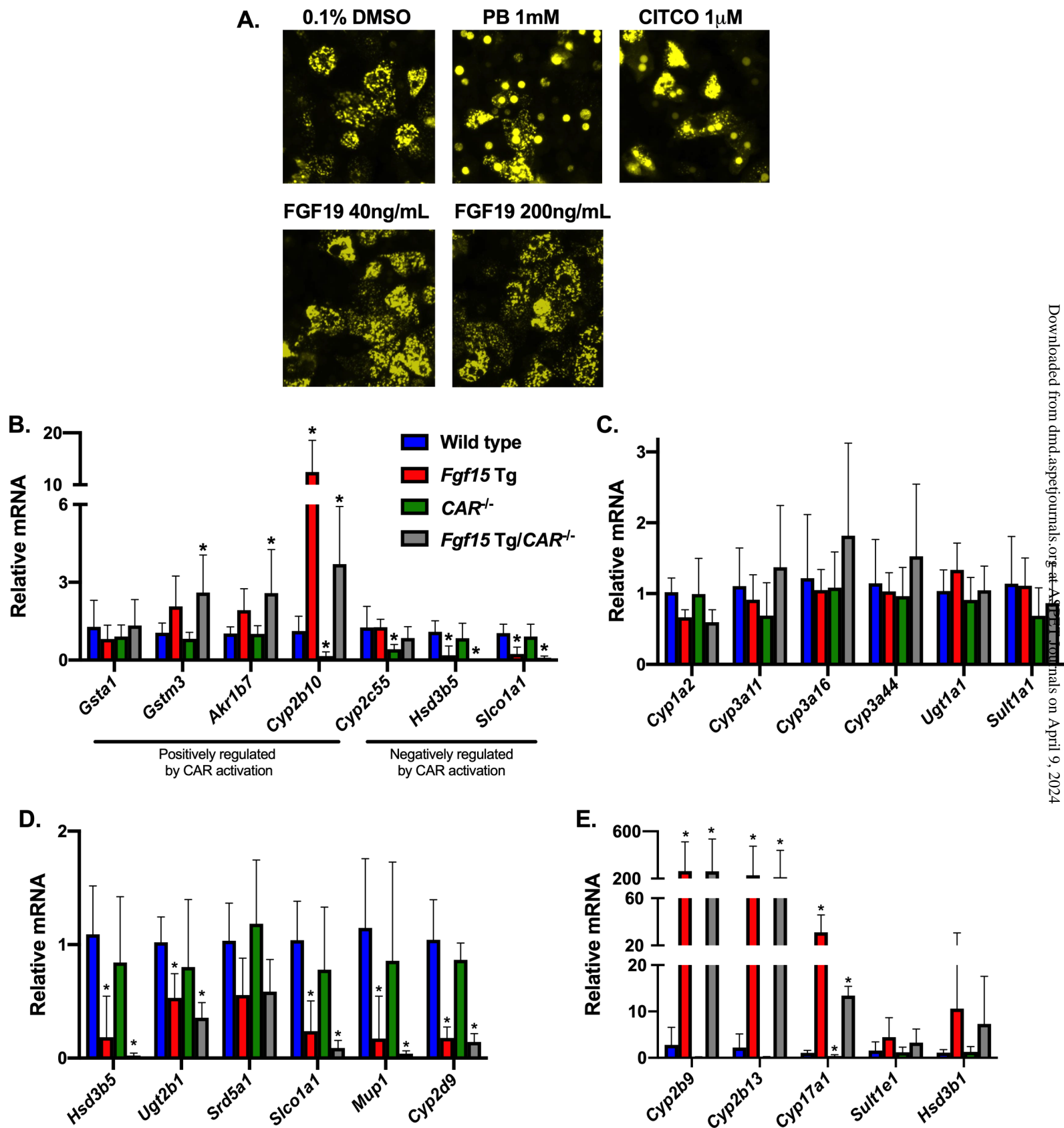
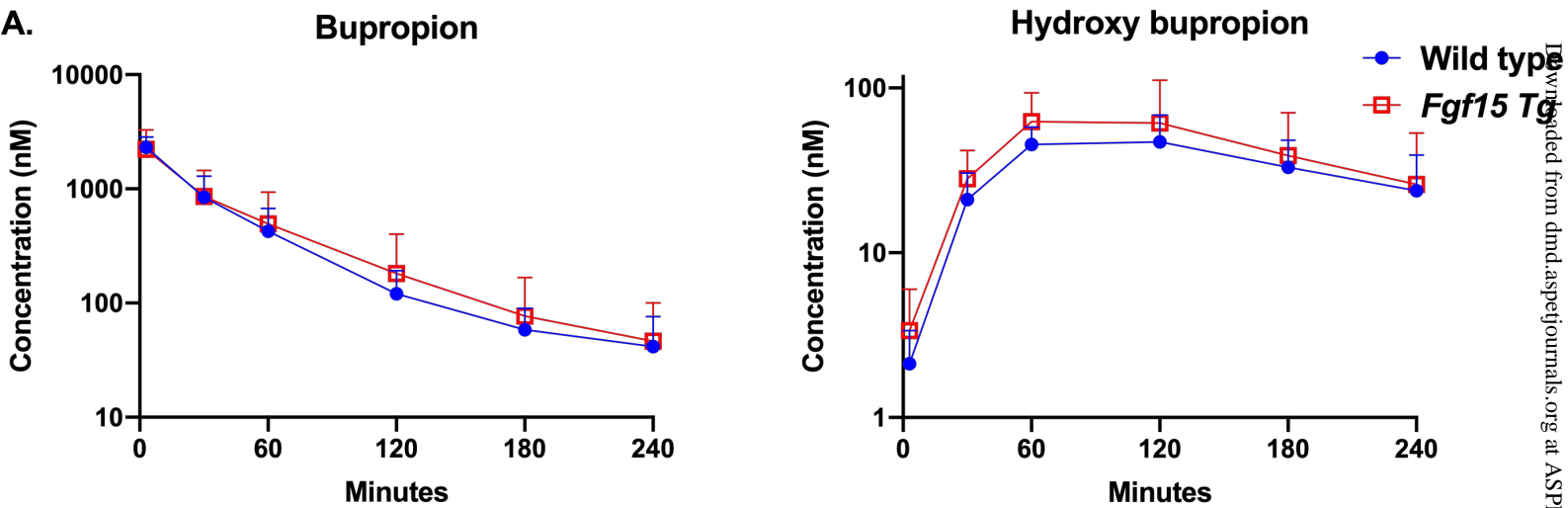


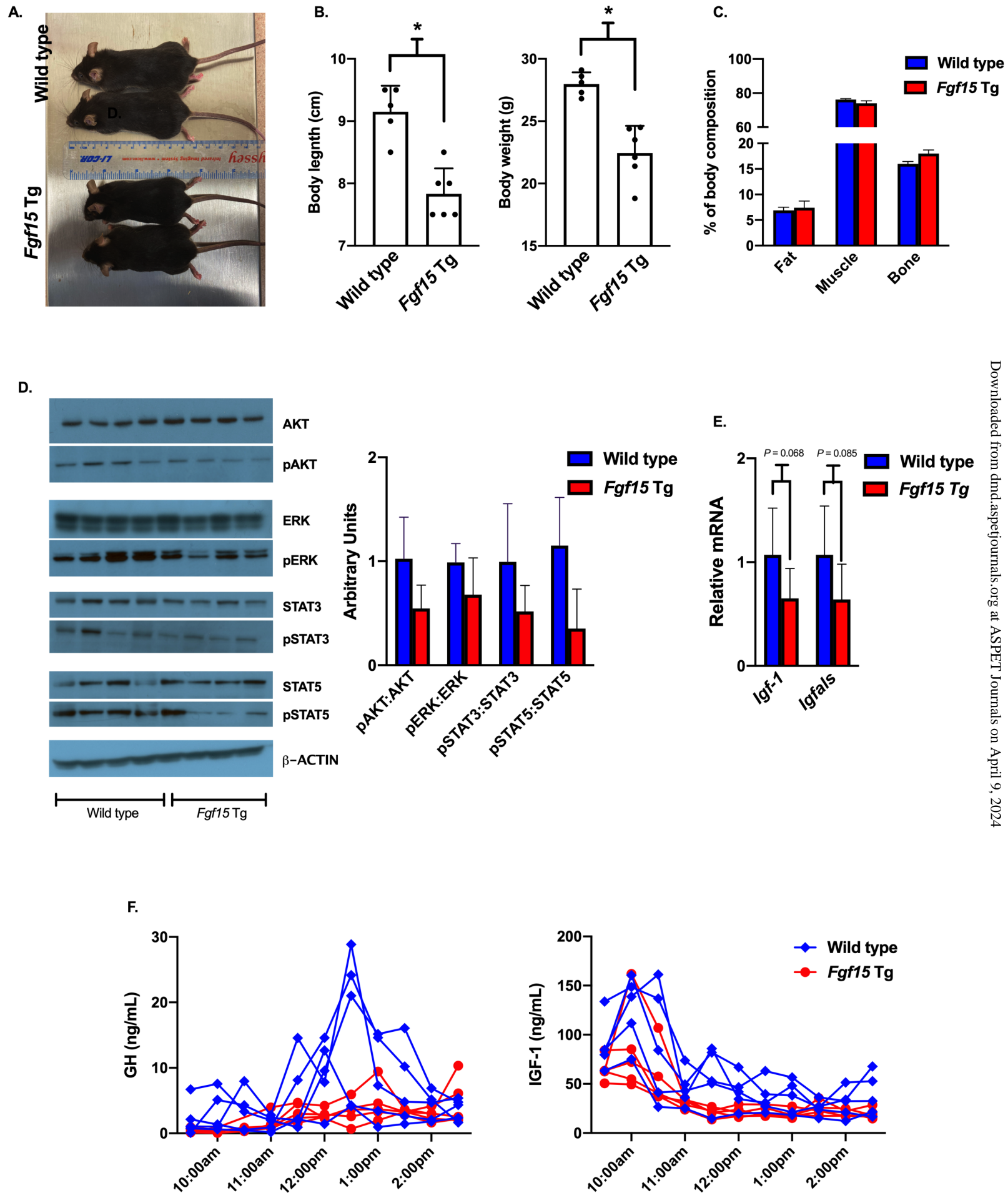
Figure 4



**B.**

Pharmacokinetic parameter	Bupropion		Hydroxybupropion	
	Wild type	<i>Fgf15 Tg</i>	Wild type	<i>Fgf15 Tg</i>
<b>AUC<sub>(0-inf)</sub>(ng/ml * min)</b>	23,320 ± 8,756	24,946 ± 15,968	3,992 ± 2,878	3,816 ± 3,055
<b>C<sub>max</sub> (ng/ml)</b>	552.5 ± 127.2	531.6 ± 254.3	13.4 ± 4.1	18.1 ± 12.6
<b>T<sub>max</sub> (min)</b>	3.0 ± 0.0	3.0 ± 0.0	96.0 ± 31.0	68.6 ± 22.7
<b>T<sub>1/2</sub> (min)</b>	55.8 ± 21.5	46.8 ± 11.3	157.9 ± 113.4	105.3 ± 54.4
<b>MRT<sub>(0-inf)</sub>(min)</b>	50.6 ± 18.6	50.1 ± 25.1	271.8 ± 167.5	194.3 ± 77.5

Figure 5



## **Supporting Information**

### **Effects of Overexpression of Fibroblast Growth Factor 15/19 on Hepatic Drug Metabolizing Enzymes**

Daniel Rizzolo, Bo Kong, Stephanie Piekos, Liming Chen, Xiaobo Zhong, Jie Lu, Jian Shi,  
Hao-jie Zhu, Qian Yang, Albert Li, Linhao Li, Hongbing Wang, Anna Siemiątkowska,  
Celine Park, Leonid Kagan, Grace L. Guo

Department of Pharmacology and Toxicology, Ernest Mario School of Pharmacy (DR, BK, GLG), Department of Pharmaceutical Sciences, Ernest Mario School of Pharmacy (AS, CP, LK), Center of Excellence for Pharmaceutical Translational Research and Education (AS, CP, LK), Environmental and Occupational Health Sciences Institute (EOHSI) Rutgers University, Piscataway, NJ 08854 (DR, GLG); Rutgers Center for Lipid Research, Rutgers, The State University of New Jersey, New Brunswick, NJ 08901 (DR, GLG); VA New Jersey Health Care System, Veterans Administration Medical Center, East Orange, NJ 07017 (GLG); Department of Pharmaceutical Sciences, University of Connecticut, Storrs, CT 06269 (SP, LC, XZ); Department of Pharmaceutical Sciences, School of Pharmacy, University of Pittsburgh, Pittsburgh, PA 15261 (JL); Department of Clinical Pharmacy, College of Pharmacy, University of Michigan, Ann Arbor, MI 48109 (JS, HZ); In Vitro ADMET Laboratories, LLC, Columbia, MD 21045 (QY, AL); Department of Pharmaceutical Sciences, School of Pharmacy, University of Maryland, Baltimore, MD 21201 (LL, HW); Department of Physical Pharmacy and Pharmacokinetics, Poznan University of Medical Sciences, Poznań 60-781, Poland (AS)



Corresponding Author: Grace L. Guo, MBBS, PhD, 170 Frelinghuysen Road, Piscataway,  
NJ, 08854 (address), (848)445-8186 (phone), (732)445-4161 (fax),  
guo@eohsi.rutgers.edu (e-mail)

Genes	Forward	Reverse
<i>Akr1b7</i>	AAGCGGGAGGATCTTTCAT	TCAGATCCGAGAGGGTGTTTC
<i>Cyp17a1</i>	TGGCTTTCTGGTGCACAATC	GGAGGTGAGTCCGGTCATTGAA
<i>Cyp1a2</i>	ACATCCTTTGTCCCTTCAC	GGTCTTTCCACTGCTTCTCATC
<i>Cyp2b10</i>	GACTTTGGGATGGGAAAGAG	CCAAACACAATGGAGCAGAT
<i>Cyp2b13</i>	GCTTTTCTACCTTCTCCACAG	ATGTCCCTTAGAAGCAACAGGG
<i>CYP2B6</i>	CGGGGATATGGTGATCTT	AGTGGTCACAGAGAATCGCC
<i>Cyp2b9</i>	TGGCCACCATGAAAGAGTTTG	GCTGTGATGCACTGGAAGAGAA
<i>Cyp2c55</i>	ATCTTGAACCTCCCATGGATG	CACTCGCCCCAAAATGTAAC
<i>Cyp2d9</i>	TGGCAGAGATAGAGAAGGCCA	TCACGCACCCCATGAGC
<i>Cyp3a11</i>	TCACAGACCCAGAGACGATTAAGA	CCCGCCGGTTTGTGAAG
<i>Cyp3a16</i>	TCACCACTGGAAATCTCAAGG	CACCTAACACATCTTTCACAGC
<i>CYP3A4</i>	AGTGGAAAACCTCAAGGAGATGG	CGATGTTCACTCCAAATGATGT
<i>Cyp3a44</i>	ACATTCACCACTGGAAAGACTC	CCTAACACATCTTTCATAGCAACAG
<i>Cyp7a1</i>	AACAACCTGCGAGTACTAGATAGC	GTGTAGAGTGAAGTCTCTTAGC
<i>Fgf15</i>	GCCATCAAGGACGTCAGCA	CTTCTCCGAGTAGCGAATCAG
<i>Fxr</i>	TCCGGACATTCAACCATCAC	TCACCTGCACATCCAGATCTC
<i>Gsta1</i>	CCCCTTTCCCTCTGCTGAAG	TGCAGCTTCACTGAATCTTGAAAG
<i>Gstm3</i>	GAAGCACAACTGCTGTGGAGA	ATCGGGACTGCAGCAGACTAT
<i>Hsd3b1</i>	ATTCCGACCAGAAACCAAGG	AGAATGTCTCCTTCCAACACTG
<i>Hsd3b5</i>	CACTAGTGAAGCAGCACAGG	AGGTTCCAGGCAATTCAGTA
<i>Mup1</i>	AAGGTTTGACAACTATGTGAGA	TCCTGGTGAGAAGTCTCCACTC
<i>Shp</i>	CGATCCTCTTCAACCCAGATG	AGGGCTCCAAGACTTCACACA
<i>Slco1a1</i>	CACTGGGAGCTTTGAGATAGG	TGAGGAAATGAGGTGATGCC
<i>Srd5a1</i>	TGTTTGCTCTGTTCACCTG	TGGACAGCACACTAAAGCAG
<i>Sult1a1</i>	GAAAGTGTCTATGGGTCGTG	CGCCCCAGAACTCTAGAATC
<i>Sult1e1</i>	AAGGGCAAGTTCCGTATGG	CTCTCCAGGAAGCTATTAGCTTTAC
<i>Ugt1a1</i>	GCTTCTCCGTACCTTCTGTTG	GCTGCTGAATAACTCCAAGCAT
<i>Ugt2b1</i>	GTGCTGGTGTGGCCTACAG	ATTGCTCGGCCAATGAGG

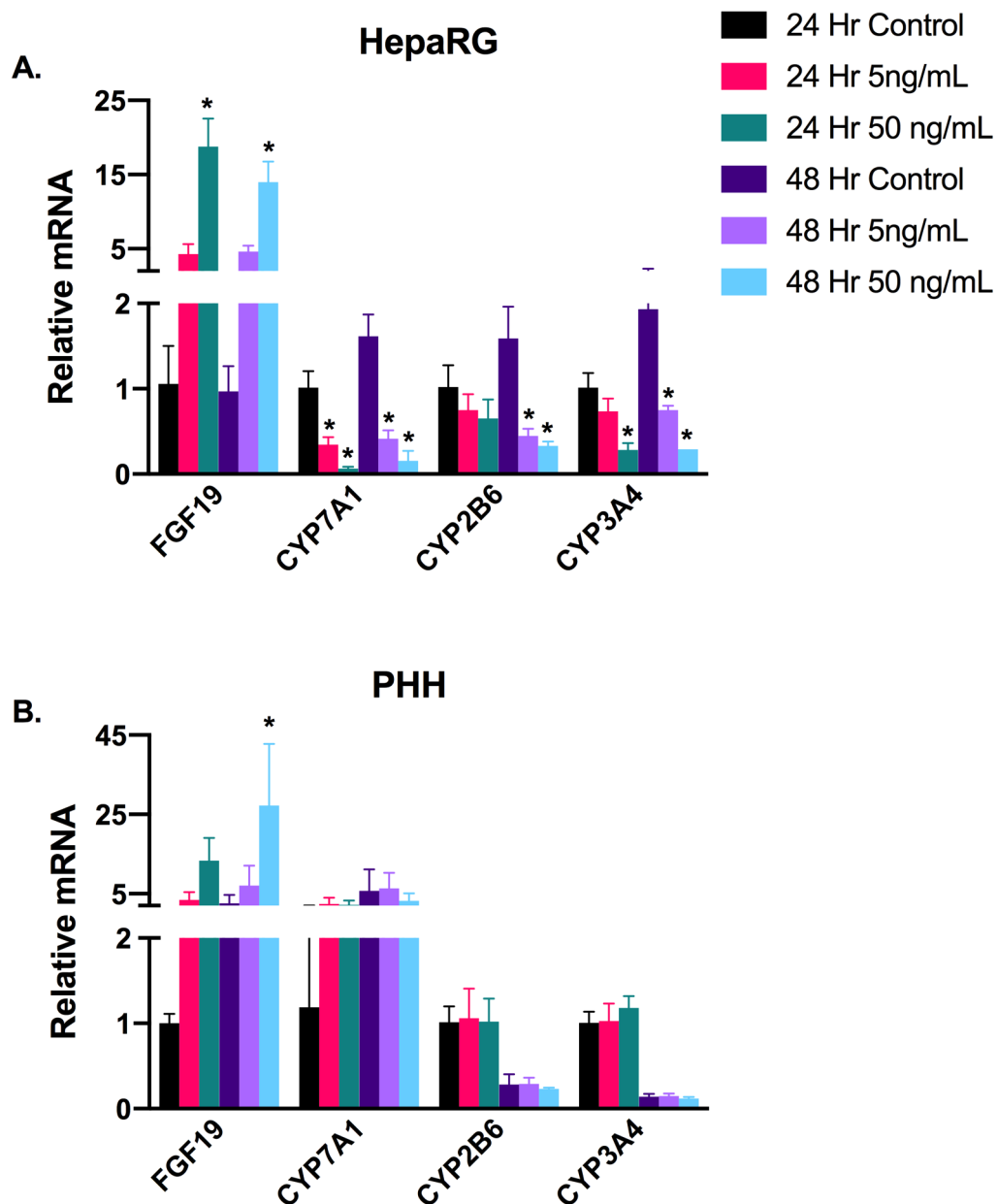
Anitbody	Manufacturer	Catalog #	Lot #
CYP2B10	EMD Millipore (Billerica, MA)	AB9916	2794496
CYP3A11	Gift from Dr. Frank Gonzalez lab (NIH)	N/A	N/A
GAPDH	EMD Millipore (Billerica, MA)	MAB374	2955484
STAT3	Cell Signaling Tech. (Danvers, MA)	4904S	7
P-STAT3	Cell Signaling Tech. (Danvers, MA)	9134S	21
STAT5a/b	R&D Systems (Minneapolis, MN)	AF2168	KVE0318111
P-STAT5	Cell Signaling Tech. (Danvers, MA)	4322S	8
ERK1/2	Cell Signaling Tech. (Danvers, MA)	9102S	26
P-ERK1/2	Cell Signaling Tech. (Danvers, MA)	4370S	24
AKT	Cell Signaling Tech. (Danvers, MA)	4691P	17
P-AKT	Cell Signaling Tech. (Danvers, MA)	13038S	7
B-ACTIN	Developmental Studies Hybridoma Bank (Iowa City, IA)	JLA20	N/A

	Number of animals	Average body weight (g)	Average liver weight (g)
<b>Wild type</b>	9	26.8	1.24
<b>CKO</b>	6	26.1	1.12
<b><i>Fgf15</i> Tg</b>	5	20.8	0.80

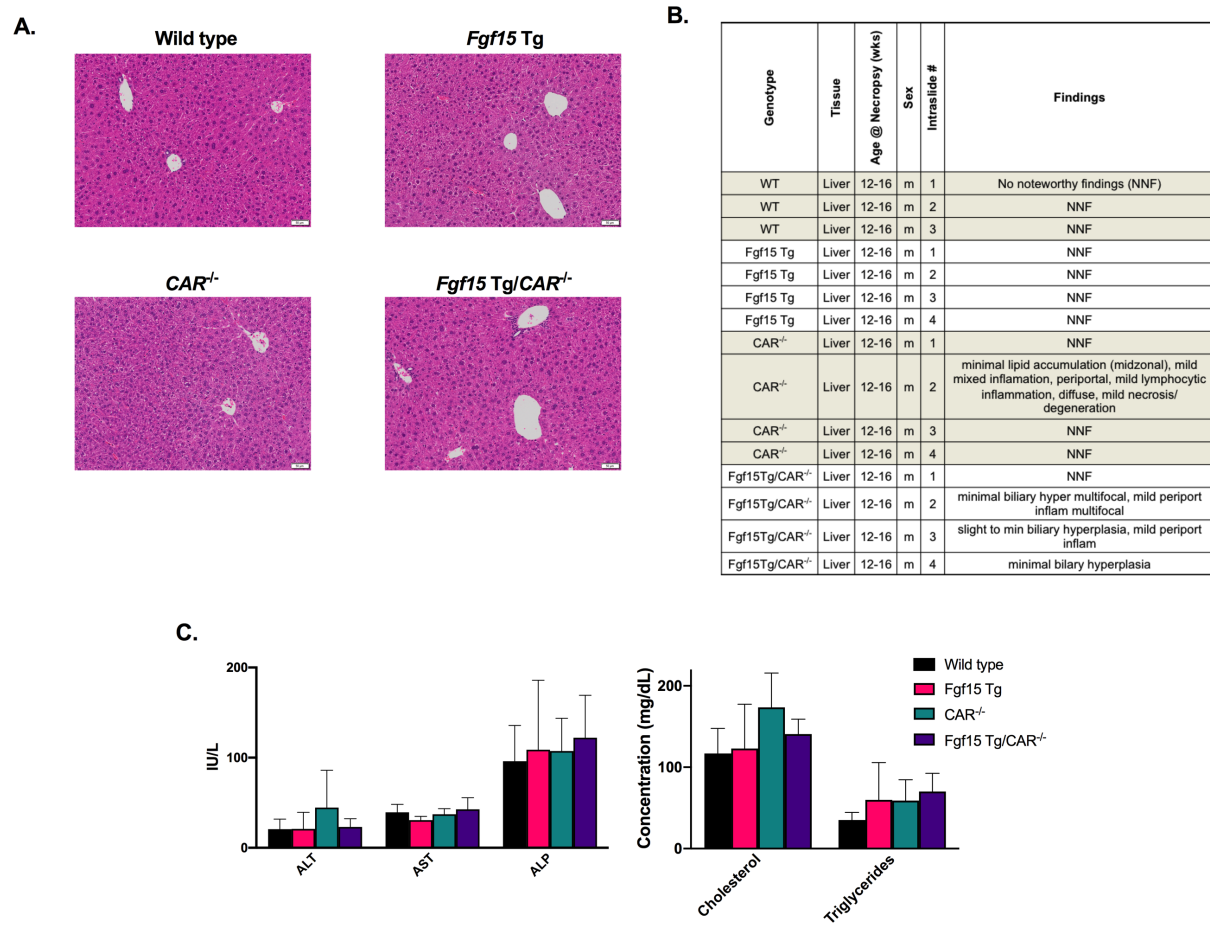
	Number of animals	Average body weight (g)	Average liver weight (g)
<b>Wild type</b>	6	26.67	1.12
<b><i>Fgf15</i> Tg</b>	7	23.44	1.01
<b>CAR<sup>-/-</sup></b>	7	27.23	1.27
<b><i>Fgf15</i> Tg/CAR<sup>-/-</sup></b>	7	22.74	1.04

	Number of animals	Average body weight (g)	Average liver weight (g)
<b>Wild type</b>	10	29.54	1.05
<b><i>Fgf15</i> Tg</b>	8	22.11	0.84

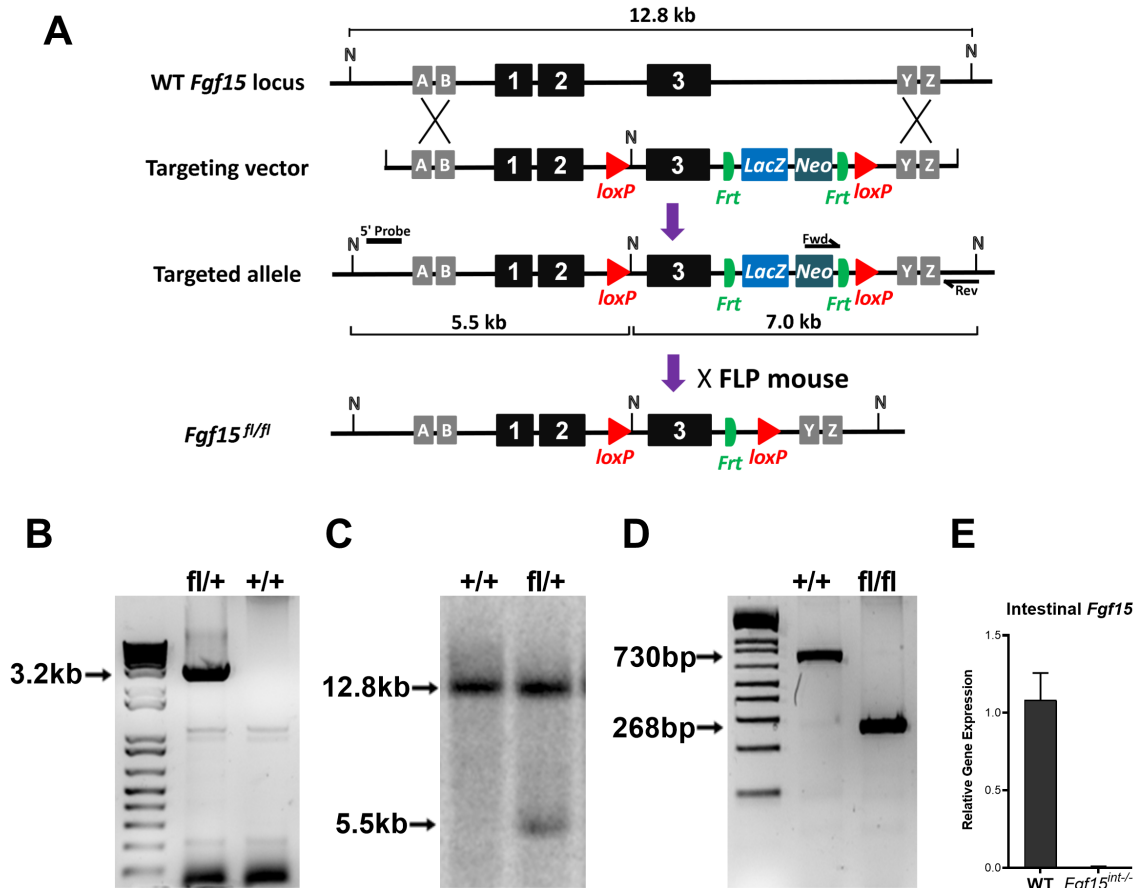
**Supplemental Fig. 1** Primer, antibody, and animal information



**Supplemental Fig. 2** *In vitro* assays showing mRNA expression of selected genes following treatment with recombinant FGF19 protein. (A) Relative mRNA in HepaRG cells following treatment with FGF19. (B) Relative mRNA in PHHs following treatment with FGF19. Graphs depict relative mRNA  $\pm$  1 SD. An asterisk denotes a significant difference from control treated samples of the same time point ( $P < 0.05$ ).

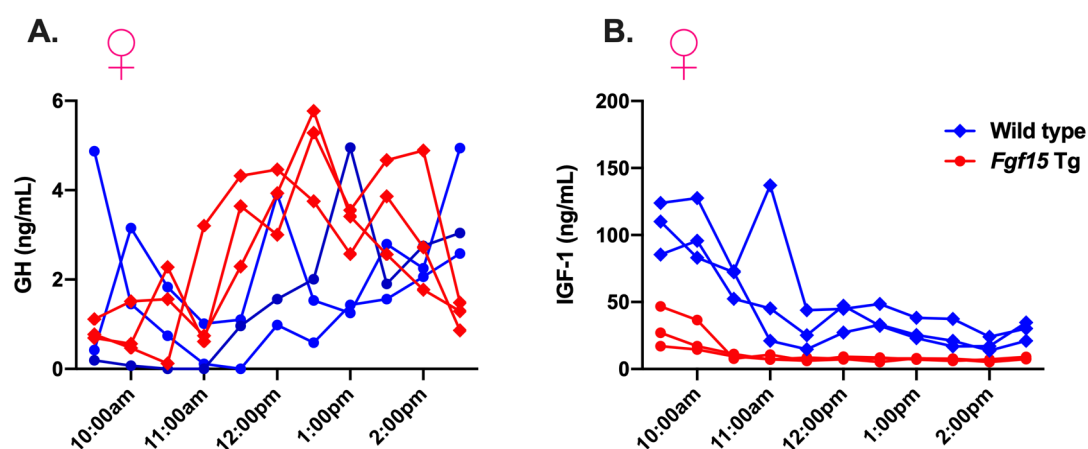


**Supplemental Fig. 3 Liver histology and function assessment.** (A) Representative images of H&E stained liver sections. (B) Chart detailing pathological findings. (C) Serum assay of triglycerides and cholesterol (mg/dL) and liver injury biomarkers AST, ALP, and ALT (IU/L).



**Supplemental Fig. 4 Generation of *Fgf15* Conditional Knockout Mice.** (A) Schematic representation of the mouse *Fgf15* locus and targeting strategy. The targeting vector was designed to contain an Frt flanked neomycin cassette, and two loxP sites flanking the 3<sup>rd</sup> exon of the *Fgf15* gene. Targeted mice are crossed to a mouse strain expressing the FLPe recombinase to delete the neomycin selection cassette. N, *NsiI*; (B) PCR analysis of *Fgf15* mutant alleles. Genomic DNA from ES cells was isolated and PCR was performed using a pair of primers, one located on the neomycin resistance cassette, and the other one located at the downstream of the recombination site; (C) Southern blot analysis of *Fgf15* mutant alleles. Genomic DNA from ES cells was digested with *NsiI* and hybridized to a 5' probe. The position of the probe is indicated; (D) PCR genotyping to distinguish modified *Fgf15* alleles. The primers produced the PCR products for the wild-type (WT) or mutant

alleles (730bp vs. 268bp); (E) Quantitative real time PCR gene expression analysis of *Fgf15* mRNA levels in the intestine confirmed the gene mutation in *Fgf15*<sup>int-/-</sup> mice.



**Supplemental Fig. 5.** Serum (A) GH and (B) IGF-1 levels for female WT and *Fgf15* Tg mice.

Protein IDs	Surrogate Peptides
Cyp2b9	R.EALVDHAEAFSGR.G
	R.FSDLVPIGLPHK.V
Cyp2b10	R.EALVGQAEAFSGR.G
	R.GTVAVVEPTFK.E
	K.ATLDPSVPR.D
	R.DFIDIYLLR.M
Cyp2b19	R.FSDLPIGVPHR.V
Cyp3a11	K.NLQEILDYIGHSVEK.H
	K.TWGLFDGQTPLAVTDPETIK.N
	R.DFGPVGIMSK.A
	K.LQDEIDEALPNK.A
Cyp3a13	R.LYPIANR.L
	K.LGIPGPKPLPFLGTILAYQK.G
	R.FGPVGILK.K
	R.ALLSPTFTSGR.L
Cyp3a16	K.QGLLQPENPLLLK.V
	R.ALLSPTFTSGNLK.E
Cyp3a25	R.ELLQPVKPIVLK.V
	R.TLLSPTFTSGK.L

**Supplemental Table 1.** Surrogate peptides used for LC-MS/MS-based protein quantification

## **Supplemental Doc. 1**

### **PK study – bupropion (BUP) and hydroxybupropion (HBUP)**

#### **Materials and methods:**

Bupropion hydrochloride (98%), bupropion-D9 hydrochloride (97%), hydroxybupropion-D6 (95%) were obtained from Toronto Research Chemicals; hydroxybupropion ( $\geq 98\%$ ) was obtained from Cayman Chemical; trichloroacetic acid ( $\geq 99\%$ ) and K<sub>3</sub>EDTA (98%) were obtained from Sigma-Aldrich, LCMS grade: methanol, acetonitrile, water, formic acid, ammonium formate were obtained from Fisher Scientific.

#### **Stock and working solutions:**

Stock solutions of BUP (1 mg/mL free base) and HBUP (1 mg/mL), as well as their corresponding internal standards: BUP-D9 (0.5 mg/mL free base) and HBUP-D6 (0.5 mg/mL) were prepared in methanol. Working solutions were prepared by further dilution of stock solutions with methanol. All stock and working solutions were kept at -20°C.

#### **Instrumentation and LC-MS/MS conditions:**

Concentrations of BUP and its major metabolite, HBUP, were determined with an LC-MS/MS method. Analysis was performed using an AB Sciex QTRAP 6500+ mass spectrometer coupled with an AB Sciex ExionLC AD system. Detection of analytes was conducted using positive electrospray ionization (ESI+) in multiple reaction monitoring (MRM) mode. The mass spectrometer was operated with an ion spray voltage of 2500 V; a source temperature of 350°C; a collision gas on medium level; gas 1, gas 2, and curtain gas of 60, 40, and 35 psi, respectively. The MRM transitions used for quantitation as well as compound-specific parameters are presented in Table 1.

**Table 1.** Acquisition parameters used in the LC-MS/MS analysis.

	<b>Q1/Q3 [m/z]</b>	<b>RT [min]</b>	<b>DP [V]</b>	<b>EP [V]</b>	<b>CE [V]</b>	<b>CXP [V]</b>
<b>BUP</b>	240.976/132.000	2.36	31	10	37	14
<b>BUP-D9</b>	250.001/132.200	2.34	36	10	39	12
<b>HBUP</b>	256.992/168.100	2.03	26	10	31	10
<b>HBUP-D6</b>	262.997/131.000	2.01	36	10	61	16

Q1 and Q3 – precursor and product ions, RT – retention time, DP – declustering potential, EP – entrance potential, CE – collision energy, CXP – collision cell exit potential, BUP – bupropion, BUP-D9 – bupropion-D9 (internal standard for BUP), HBUP – hydroxybupropion, HBUP-D6 - hydroxybupropion-D6 (internal standard for HBUP)

The LC separation was performed at 45°C on a Phenomenex Luna Omega PS C18 column (50 x 2.1 mm ID, particle size 3 µm) protected by a SecurityGuard Cartridges PS C18 (4 x 2.0mm ID). The aqueous mobile phase (MPA) consisted of 10 mM ammonium formate and 0.1% formic acid in water; the organic mobile phase (MPB) consisted of acetonitrile. The mobile phase was pumped at a flow rate of 0.6 mL/min with a gradient profile as follows: 0 – 0.5 min, 5% MPB; 0.5 – 2.6 min, 5 – 33% MPB; 2.6 – 3.2 min, 33 – 95% MPB; 3.2 – 4.0 min, 95% MPB; 4.0 – 4.5 min, 95 – 5% MPB; 4.5 – 5.5 min, 5% MPB. The temperature of the autosampler was maintained at 15°C. After each injection, the autosampler was washed with two rinsing solvents: R0 – a mixture of acetonitrile and water (50/50, v/v) with 0.1% formic acid (used for external rinsing) and R1 – a mixture of isopropanol, acetonitrile, methanol, and water (25/25/25/25, v/v/v/v) (used for internal rinsing).



**Sample preparation:**

After thawing at room temperature, 10 µL of mouse K<sub>3</sub>EDTA plasma was spiked with 10 µL of a mixture of internal standards (250 ng/mL HBUP-D6 and 1000 ng/mL BUP-D9 in MeOH) and 10 µL of 10% trichloroacetic acid. Samples were vortexed for 5 min and centrifuged for 5 min at 10°C with 15 700 x *g*. The resulted supernatant was filtered through 0.2 µm PVDF filters at 10°C. The filtrate was then transferred to the HPLC vials with high-recovery inserts, and 10 µL was injected into the column.

## **CYP2B and CYP3A enzyme activity**

Liver microsomes were isolated from liver tissue, as previously described (Tien et al., 2015). Pentoxyresorufin and midazolam were used as probe substrates for the reactions pentoxyresorufin O-dealkylation and midazolam 1'-hydroxylation, which was used to detect the enzymatic activities of CYP2B and CYP3A, respectively. In brief, protein concentrations of isolated microsomes were measured using Modified Lowry Protein Assay Kit (Thermo Fisher Scientific Inc., Rockford, IL). The incubation of 50µg of mouse liver microsomes was carried out in 1x phosphate-buffered saline (pH 7.4) with 30µM substrate concentration in a total volume of 95µL. The reactions were initiated with 5µL of 20mM NADPH. Reactions containing pentoxyresorufin were carried out for 30 minutes and reactions containing midazolam were carried out for 10 minutes. All reactions were terminated by the addition of 100µL of ice-cold acetonitrile. The samples were vortexed for 30 seconds, centrifuged at 15,000rpm for 10 minutes, and 1.0µL aliquots of the supernatant were injected into Waters Synapt G2-S QTOFMS system (Waters, Milford, MA) for metabolite analysis. Chromatographic separation of metabolites was performed on an Acquity UPLC BEH C18 column (2.1 × 100 mm, 1.7 µm, Waters). The mobile phase A (MPA) was 0.1% formic acid in water, and mobile phase B (MPB) was 0.1% formic acid in acetonitrile. The gradient for aqueous extraction began at 5% MPB and held for 0.5 min, followed by 5-min linear gradient to 95% MPB, held for 2 min and decreased to 5% MPB for column equilibration. The flow rate of mobile phase was 0.50 ml/min and the column temperature was maintained at 50 °C. The G2-S QTOFMS system was operated in resolution mode (resolution ~ 20,000) with electrospray ionization. The source and desolvation temperatures were set at 150 and 500 °C, respectively. Nitrogen was applied as the cone gas (50 l/h) and desolvation gas (800 l/h). The capillary and cone voltages were set at 0.8 kV and 40 V. The data were

acquired in positive ionization mode. QTOFMS was calibrated with sodium formate and monitored by the intermittent injection of lock mass leucine enkephalin ( $m/z = 556.2771$ ) in real time. Quanlynx software (Waters, Milford, MA) was used for the quantification of the concentrations of metabolites.

## **LC-MS/MS-based protein quantification**

### *Chemicals and Reagents*

Dithiothreitol, urea and water with 0.1% formic acid were purchased from Fisher Scientific (Pittsburgh, PA). Acetonitrile, formic acid, and trifluoroacetic acid were obtained from Sigma-Aldrich (St. Louis, MO). Acetonitrile with 0.1% formic acid was obtained from J.T. Baker Chemical Company (Phillipsburg, NJ). Ammonium bicarbonate and iodoacetamide were the products of Acros Organics (Morris Plains, NJ). TPCK-treated trypsin was obtained from Worthington Biochemical Corporation (Freehold, NJ). Lysyl endopeptidase was purchased from Wako Chemicals (Richmond, VA). Water Oasis HLB columns were from Waters Corporation (Milford, MA). Bovine serum albumin (BSA) standard was purchased from Thermo Fisher Scientific (Waltham, MA). All other chemicals were of analytical grade and commercially available.

### *Proteomic sample preparation*

Mouse liver microsome samples were digested for LC-MS/MS-based proteomics analysis using a previously published method (Shi et al. 2009). Briefly, aliquots of 80 µg proteins from liver microsomes were mixed with 0.2 µg of BSA internal standard. The protein mixture was precipitated with a 10-fold volume of pre-cooled acetone. The precipitated proteins were air-dried after the removal of the supernatant. The dried proteins were resuspended in 100 µL of 8 M urea solution containing 4 mM dithiothreitol and 100 mM ammonium bicarbonate and incubated at 37°C for 45 min for reduction. After samples were cooled down to room temperature, 100 µL 20 mM iodoacetamide solution in 8 M urea/100 mM ammonium bicarbonate was added for alkylation at room temperature in the dark. The urea concentration was then adjusted to 6 M by adding 50 mM ammonium bicarbonate solution. Lysyl endopeptidase (Wako Chemical) was added for the first

digestion step (protein to enzyme ratio 100:1) at 37°C for 6 hours. The urea concentration was further reduced to 1.6 M using 50 mM ammonium bicarbonate solution, followed by the second digestion step with TPCK-treated trypsin at a protein to enzyme ratio of 50:1 at 37°C overnight. Digestion was terminated by adding 1 µL trifluoroacetic acid. Digested peptides were extracted and purified using Waters Oasis HLB columns (Waters Corporation, Milford, MA) according to the manufacturer's instructions. The eluted peptides were dried in a Speed Vac SPD1010 (Thermo Scientific, Hudson, NH) and reconstituted in 80 µL 3% acetonitrile containing 0.1% formic acid. The peptide samples were centrifuged and supplemented with synthetic iRT standard solutions (Biognosys AG, Cambridge, MA) prior to LC-MS analysis.

#### *LC-MS/MS-based protein quantification*

The digested peptide samples were analyzed on a TripleTOF 5600+ mass spectrometer (AB Sciex, Framingham, MA) coupled with an Eksigent 2D plus LC system (Eksigent Technologies, Dublin, CA). LC separation was performed via a trap-elute configuration including a trapping column (ChromXP C18-CL, 120 Å, 5 µm, 10 × 0.3 mm, Eksigent Technologies, Dublin, CA) and an analytical column (ChromXP C18-CL, 120 Å, 150 × 0.3 mm, 5 µm, Eksigent Technologies, Dublin, CA). The mobile phase consisted of water with 0.1% formic acid (phase A) and acetonitrile with 0.1% formic acid (phase B). A total of 6 µg protein was injected for analysis. Peptides were trapped and cleaned on the trapping column with mobile phase A delivered at a flow rate of 10 µL/min for 3 min before being separated on the analytical column with a gradient elution at a flow rate of 5 µL/min. The gradient time program was set as follows (mobile phase B): 0 to 68 min: 3% to 30%, 68 to 73 min: 30% to 40%, 73 to 75 min: 40% to 80%, 75 to 78 min: 80%, 78 to 79 min: 80% to 3%, and 79 to 90 min: 3%. The TripleTOF instrument was operated in a positive

ion mode with an ion spray voltage floating at 5500 v, ion source gas one at 28 psi, ion source gas two at 16 psi, curtain gas at 25 psi, and source temperature at 280°C. A blank injection after each sample was used to prevent carryover.

The digested microsomes samples were analyzed using a sequential window acquisition of all theoretical mass spectra (SWATH) method comprised of a 250 ms TOF-MS scan from 400 to 1250 Da, followed by MS/MS scans from 100 to 1500 Da performed on all precursors in a cyclic manner. The accumulation time was 50 ms per isolation window, resulting in a total cycle time of 2.8 s. The spectral alignment and target data extraction of the SWATH data were performed on Skyline-daily (version 3.7.1.11271, University of Washington, Seattle, WA) with the reference spectral library generated from an in-house information-dependent acquisition search. The isolation scheme in Skyline-daily was set as “SWATH (VW 100)”. The MS1 and MS/MS filtering were both set as “TOF mass analyzer” with the resolution power of 30,000 and 15,000, respectively. The retention time prediction was based on the auto-calculate regression implemented in the iRT calculator. Proper peak selection was checked manually with the automated assistance of Skyline-daily. The surrogate peptides used for the quantification of CYP2B9, CYP2B10, CYP2B19, CYP3A11, CYP3A13, CYP3A16, CYP3A25 were listed in Supplemental Table 1. These peptides were selected based on their uniqueness and chromatographic performance. The peak areas of top 3 to 5 fragment ions were summed up and normalized to the internal standard BSA. The BSA-normalized peak area of each peptide was further divided by the average of the 18 samples to calculate the relative abundance of the peptide. The average of relative abundance of all surrogate peptides of a protein was used to determine the relative abundance across different microsome samples.

## Generation of *Fgf15* Conditional Knockout Mice

The targeting vector for intestinal *Fgf15* specific knockout mouse (*Fgf15<sup>int-/-</sup>*) was generated using homologous recombination method (Liu et al., 2003). Briefly, 12.8 kb of genomic fragment containing all three exons of the *Fgf15* gene was amplified by PCR and subcloned into the pL253 plasmid as depicted in **Suppl. Fig. 4A**. Two loxP sites were subcloned subsequently by Red/ET recombineering into the introns flanked exon 3, which encodes the domains that mediate HSPG and FGFR binding interactions (Wright et al., 2004). The final targeting vector comprises three *Fgf15* exons, two loxP sites, a bovine growth hormone polyadenylation signal (bGHpA), and a FLP recognition target-flanked neomycin expression cassette, shown in **Suppl. Fig. 4A**.

The targeting vector was linearized with *NotI* and electroporated into murine 129SvJ mouse embryonic stem cells (NCI Genome Modification Core). After selection with G418, the cells were screened by PCR for the desired modification using a forward primer located at the Neo cassette (5'-ATCGCCTTCTATCGCCTTCTTGACGAGTTC-3') and a reverse primer located at 3' end of the *Fgf15* gene (5'- ATGCAGTACCCGAGGAGGC-3'), which amplifies a fragment from the new junction created by homologous recombination at the 3' end of *Fgf15* gene (**Suppl. Fig. 4B**). The colonies were further confirmed for the correctly targeted 5' homology arms by standard Southern blot analyses (**Suppl. Fig. 4C**).

Embryonic stem cells that contained the modified *Fgf15* allele were expanded and injected into host mouse blastocysts and transferred into foster mothers. The resulting highly chimeric mice were mated with C57BL/6J mice (Jackson Laboratory, Bar Harbor, ME) to obtain germline transmission. The neomycin selection cassette in the heterozygous mice was removed *in vivo* by FLP-mediated deletion (Jackson Laboratory,

Stock 011065). Heterozygous mice without neomycin cassette were further bred with C57BL/6J mice for 10 generations to bring them to a C57BL/6 genetic background and the homozygous loxP mice (*Fgf15<sup>fl/fl</sup>*) were obtained by heterozygous intercrosses.

Genotyping by PCR using primers FGF15CKO\_Flox\_F 5'-

GAGGAGTTGCGGATTATCCGGCAG-3' and FGF15CKO\_Flox\_R 5'-

TGGCTCATCCCAGAAGTATCCAGC produced 730bp and 268bp fragments for WT and

floxed alleles, respectively (**Suppl. Fig 4D**). *Fgf15<sup>int-/-</sup>* mice were generated by crossing to

a transgenic strain carrying the villin-promoter controlled Cre and intestinal Fgf15

specific deletion were confirmed by real-time PCR (**Suppl. Fig. 4E**).